49. THERMAL CONDUCTIVITY OF SEDIMENTS AND IGNEOUS ROCKS RECOVERED DURING DEEP SEA DRILLING PROJECT LEG 60[1]

Ki-Iti Horai, Lamont-Doherty Geological Observatory of Columbia University, Palisades, New York

ABSTRACT

A total of 1547 thermal conductivity values were determined by both the NP (needle probe method) and the QTM (quick thermal conductivity meter) on 1319 samples recovered during DSDP Leg 60. The NP method is primarily for the measurement of soft sedimentary samples, and the result is free from the effect of porewater evaporation. Measurement by the QTM method is faster and is applicable to all types of samples—namely, sediments (soft, semilithified, and lithified) and basement rocks. Data from the deep holes at Sites 453, 458, and 459 show that the thermal conductivity increases with depth, the rate of increase ranging from (0.18 mcal/cm s °C)/100 m at Site 459 to (0.72 mcal/cm s °C)/100 m at Site 456. A positive correlation between the sedimentary accumulation rate and the rate of thermal conductivity increase with depth indicates that both compaction and lithification are important factors. Drilled pillow basalts show nearly uniform thermal conductivity. At Site 454 the thermal conductivity of one basaltic flow unit was higher near the center of the unit and lower toward the margin, reflecting variable vesicularity. Hydrothermally altered basalts at Site 456 showed higher thermal conductivity than fresh basalt because secondary calcite, quartz, and pyrite are generally more thermally conductive than fresh basalt. The average thermal conductivity in the top 50 meters of sediments correlates inversely with water depth because of dissolution of calcite, a mineral with high thermal conductivity, from the sediments as the water depth exceeds the lysocline and the carbonate compensation depth. Differences between the Mariana Trench data and the Mariana Basin and Trough data may reflect different abundances of terrigenous material in the sediment. There are remarkable correlations between thermal conductivity and other physical properties. The relationship between thermal conductivity and compressional wave velocity can be used to infer the ocean crustal thermal conductivity from the seismic velocity structure.

INTRODUCTION

Thermal conductivity measurements of samples collected during the Deep Sea Drilling Project have been made by a number of investigators. The primary purpose of these measurements was to calculate heat flow by combining the thermal conductivity with the temperature gradient determined for the holes. In addition to the determination of heat flow, Leg 60 thermal conductivity data were used (1) to define the thermal conductivity of seafloor sediments as a function of depth and (2) to compare the thermal conductivity with other physical properties such as porosity, water content, bulk density, and compressional wave velocity measured aboard ship.

Measurements at Sites 453, 454, 456, 458, and 459 provided useful downhole temperature data. A geometrical mean of the thermal conductivities corrected for the effects of *in situ* temperature and pressure was used in the heat flow calculation (Uyeda et al., this volume).

During Leg 60 a total of 1547 thermal conductivity values were determined on 1319 samples. Besides the conventional needle probe apparatus, the quick thermal conductivity meter, a commercially available measuring instrument using the half-space probe method, was particularly useful in processing a large number of samples. Thermal conductivity versus depth profiles was delineated for all Leg 60 holes in which thermal conductivity measurements were possible.

For all types of ocean crust samples[2] intergranular thermal contact appears to be the most important factor controlling the thermal conductivity. The total effective cross section of thermal contact between the mineral grains increases with the particle concentration. Accordingly, strong correlations are expected between the thermal conductivity and the porosity, water content, and bulk density, all of which are closely related to the particle concentration of the sample. The particle concentration also has a strong effect on the velocity of the compressional elastic wave. A relation between the thermal conductivity and the compressional wave velocity, established by experimental data, will be useful in inferring the thermal conductivity of ocean crust from the velocity structure as determined by seismic refraction.

MEASUREMENT METHODS

Needle Probe (NP)

Measurements by the method originated by Von Herzen and Maxwell (1959) were made using a probe (Fenwal Electronics G874D Series 1, 57.2 mm long and 0.86 mm in diameter, total resistance of 300 Ω energized by a DC voltage of 10.0 V) after the drilled cores were split and their temperature had reached equilibrium with that of the laboratory. Preliminary thermal conductivity values determined aboard ship were the result of quick computation using only two data points from the record of probe temperature taken continuously for 160 s. These preliminary thermal conductivity values were refined on land by reading more data points from the record and by processing them with a computer. For most of the samples, the refined thermal conductivity

[1] *Initial Reports of the Deep Sea Drilling Project*, Volume 60.

[2] Throughout the chapter "ocean crust samples" will mean samples of soft sediment, semilithified and lithified sediments, and the rock from basement.

value was within 5% of the result of the quick computation. Only the refined values will be used in the following discussion.

The NP method, although most suitable for the measurement of soft sedimentary samples, was used also on some semilithified and lithified samples. For insertion of the probe into the semilithified samples, a hole with the same length and diameter as the probe was drilled into the sample with a hand drill. For the lithified sedimentary samples that were too hard to be drilled, a groove the same width and depth as that of the probe was cut, with the aid of stainless steel wire, on the split flat surface of the sample, which was lapped smooth. The needle probe was then embedded in the groove and covered by a second split sample whose flat surface had also been lapped smooth. In order for the composite sample used in this measurement to be regarded as a homogeneous material, the two pieces had to be identical in physical properties. Usually, in the split core, two adjacent pieces of similar lithology were selected. In both these types of measurement, no special contact material was used, since the heat exchange between the probe and the sample was guaranteed by the presence of water. A total of 344 thermal conductivity values were determined by the needle probe technique; 56 of these values were determined using the second special method.

Quick Thermal Conductivity Meter (QTM)

On Leg 60 a large number of thermal conductivity measurements were made using a quick thermal conductivity meter (Sumikama and Arakawa, 1976). The measuring probe consists of a line heat source and a temperature sensor attached to a flat, smooth surface of thermally insulating material. The probe is placed on a sample and the heat source is energized by a constant DC voltage. As with the NP measurement, the probe temperature increases with time at a rate related to the sample's thermal conductivity. The measuring instrument, Showa Denko Company's Shotherm QTM, is equipped with a digital electronic circuit which computes conductivity from the temperature data with the aid of an empirical formula that is similar in functional form to that used in the NP data analysis. The formula contains two numerical constants that have been determined from the measurements on several standard materials of known thermal conductivity. Two different sets of constants are in use. The instrument's high mode of operation selects constants that are good for thermal conductivity values higher than 0.56 mcal/cm s °C. Measurement of oceanic soft sediment samples by the low mode of operation led to systematically low thermal conductivity values. The result of such measurements on all 30 samples from Site 452 and the first 23 samples from Hole 453 were corrected by an empirical formula that was derived from simultaneous measurements by both modes on the subsequent 24 samples from Hole 453:

$$k_H = (1.12 \pm 0.22)k_L + (0.08 \pm 0.09), \tag{1}$$

where both k_H and k_L, in mcal/cm s °C, are the thermal conductivities determined, respectively, with the high and low modes of operation. The QTM probe's rate of heat emission varies from 0.0047 cal/cm s to 0.075 cal/cm s, intermediate rates being appropriate for the measurement of thermal conductivity of ocean crust samples. Sample heating time is also adjustable to 20, 30, or 40 s. We chose the longest heating time for the measurement of sedimentary samples and the shortest for some hard rock samples, the surfaces of which are smaller than the probe contact area (4 cm × 10 cm). The maximum sample temperature increase was 15°C, considerably higher than the temperature disturbance given by the NP measurement, which is usually less than 3°C.

Thermal contact between the probe and the sample is the most crucial factor controlling the results of QTM measurements. To insure a steady, uniform thermal contact at the probe/sample interface, a 1000-g weight is placed on the probe which, in addition to the probe's own weight of 550 g, imposes a uniaxial pressure of 38.8 g/cm^2 during the measurement. A knife blade is adequate to produce a flat, smooth contact surface on soft sediment samples. Diffusion of the pore water maintains a perfect heat exchange between the sample and the probe. A lapping wheel was used to remove the irregularities on the split flat surface of the hard rock.

To simulate the *in situ* ocean crust condition of hard rock samples, a small amount of water was added, prior to the thermal conductivity measurement, to the probe/sample interface. Data presented in Figure 1 illustrate the effect of water on the result of the QTM thermal conductivity measurement. The data are from Hole 459B measured at 5-min intervals following the QTM probe placement on the samples. The thermal conductivity is lower for the first, reaches the maximum for the second or the third, and decreases monotonically for subsequent measurements. This is probably caused by evaporation of interfacial water. The first measurement indicates an excessive amount of water. Water, though one of the most thermally conductive materials among inorganic liquids, has a lower thermal conductivity than most of the common rock-forming minerals. Therefore an excessively thick water film increases the thermal resistance across the probe/sample interface. The maximum thermal conductivity for the second or the third measurement indicates that the amount of interfacial water becomes optimum within 5 to 10 min after the placement of the QTM probe. Subsequent decrease of thermal conductivity is due to deficiency of the interfacial water. Probably, the intrinsic thermal conductivity of the sample is closest to the maximum that was selected at Sites 459, 460, and 461. This selective criterion was not discovered until Hole 459B. Only a single measurement was made on samples from previous holes. It is unlikely, however, that the result of the single determination deviates by more than 10% from the most representative thermal conductivity value. As shown by the data in Figure 1, the thermal conductivity values, determined within 20 min after probe placement on the sample, are not more than 7% less than the maximum.

The QTM instrument is equipped with a set of standard materials: quartz glass, acrylic resin, and polyethylene foam with thermal conductivities 3.22, 0.544, and 0.116 mcal/cm s °C, respectively, at ordinary temperature (~23°C). Measurements on these standard samples were made immediately after the beginning and before the end of the cruise. Separated by a time span of 45 days, the measurements revealed a considerable drift in the lower thermal conductivity range. Figure 2 shows a satisfactory agreement for the quartz glass sample. The measurements disagreed, however, by factors of 1.64 and 7.56, respectively, for the acrylic resin and the polyethylene foam samples. The cause of the drift is likely to be in the probe. The contact surface of the QTM probe used in this study was wrapped with a thin polyimide sheet to protect the permeable probe material (an asbestos paper pile) from the moisture of the wet sample. It is conceivable that the probe cover, worn by too many measurements, invalidated the calibration. The change in the thermal resistance across the probe/sample interface, due to thinning of the probe cover, must have significantly influenced the lower mode of thermal conductivity measurement, since it is extremely sensitive to small variations in temperature. It was assumed that a majority of Leg 60 thermal conductivity values were free from the effect of the instrumental drift, since they are higher than the thermal conductivity of the quartz glass sample. A correction was made for a small number of samples, having thermal conductivities lower than the quartz glass standard. The maximum amount of correction was 6%.

Comparison of the Methods

The thermal conductivities of 228 soft sediment samples were measured by both the NP and the QTM. The two types of measurements on a continuous core, separated by no more than 5 cm, were regarded as having been made on the same sample. The results of the two measurements did not agree as well as expected. The QTM tends to give a higher thermal conductivity than the NP. The average and standard deviation for all thermal conductivity values determined by the NP are 2.44 ± 0.23 mcal/cm s °C, whereas those for the QTM are 2.75 ± 0.47 mcal/cm s °C. A weak correlation (correlation coefficient $r = 0.45$) suggests that instrument bias is not likely a cause of the systematic difference between the two measurements. A more plausible explanation would be the effect of porewater evaporation. The QTM determination of thermal conductivity is made on the split surface of the sample, exposed to the atmosphere, where the evaporation takes place. The measurement is influenced by porewater depletion, which increases the thermal conductivity of soft sediments. The NP measurement is less affected by the evaporation, since the thermal conductivity is determined in the interior of the sample where the porewater remains nearly undisturbed. No attempt has been made, however, to correct the result of the QTM measurement, since it is difficult to estimate the amount of porewater lost by evaporation.

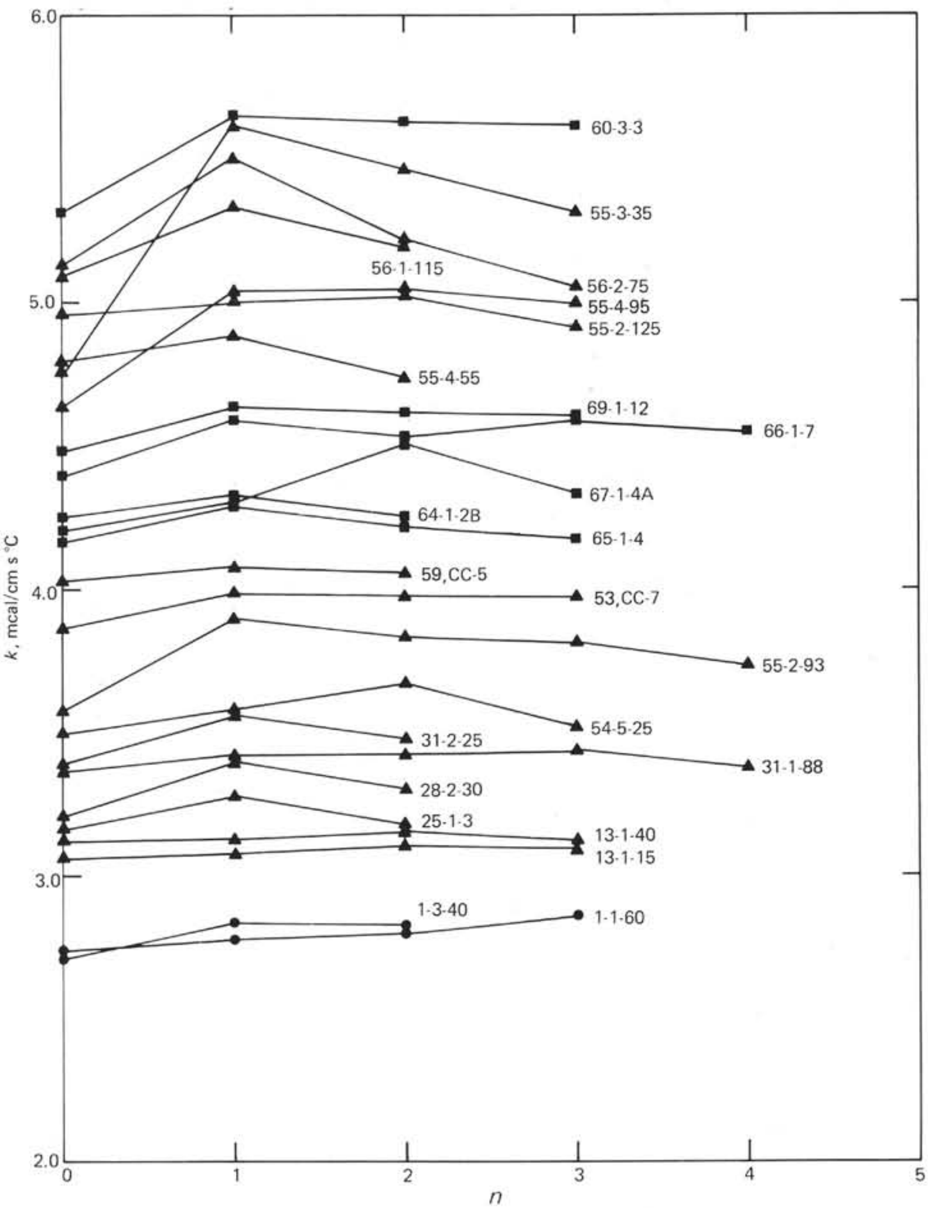

Figure 1. Thermal conductivity of Site 459 ocean crust samples determined by the QTM, plotted as a function of time. Time interval between the measurements is 5 min. The data for $n = 0$ is the result of the first measurement after the QTM probe placement on the sample. (For all figures except 2 and 12 ● = the soft sediment samples, ▲ = semilithified and lithified sediment samples, ■ = the hard rock samples from the basement.)

MEASUREMENT RESULTS

The values of thermal conductivity reported in this chapter were obtained under ordinary laboratory condition of temperature (23 ± 2°C) and pressure (1 atm). In many of the previous DSDP heat flow studies, Erickson's (1973) formula, summarized from Ratcliffe's (1960) experimental data, was used to correct the result of laboratory measurement for the effect of *in situ* temperature and pressure. The correction is valid for the samples near the tops of holes. For deeper samples, however, the formula is inadequate, because in Ratcliffe's estimate only the effect of hydrostatic pressure on each of the solid (mineral grains) and liquid (seawater) phases was considered. The effect of the uniaxial pressure from the weight of the overlying sedimentary strata on intergranular thermal contact, which becomes more important with the increasing depth, has not been taken into account. We are waiting for a more satisfactory correction procedure before applying a correction to the present thermal conductivity data. Readers are free to apply any working correction procedures to convert the laboratory thermal conductivity value to an *in situ* value. The constants and variables necessary for the conversion can be found in this and other chapters in this volume.

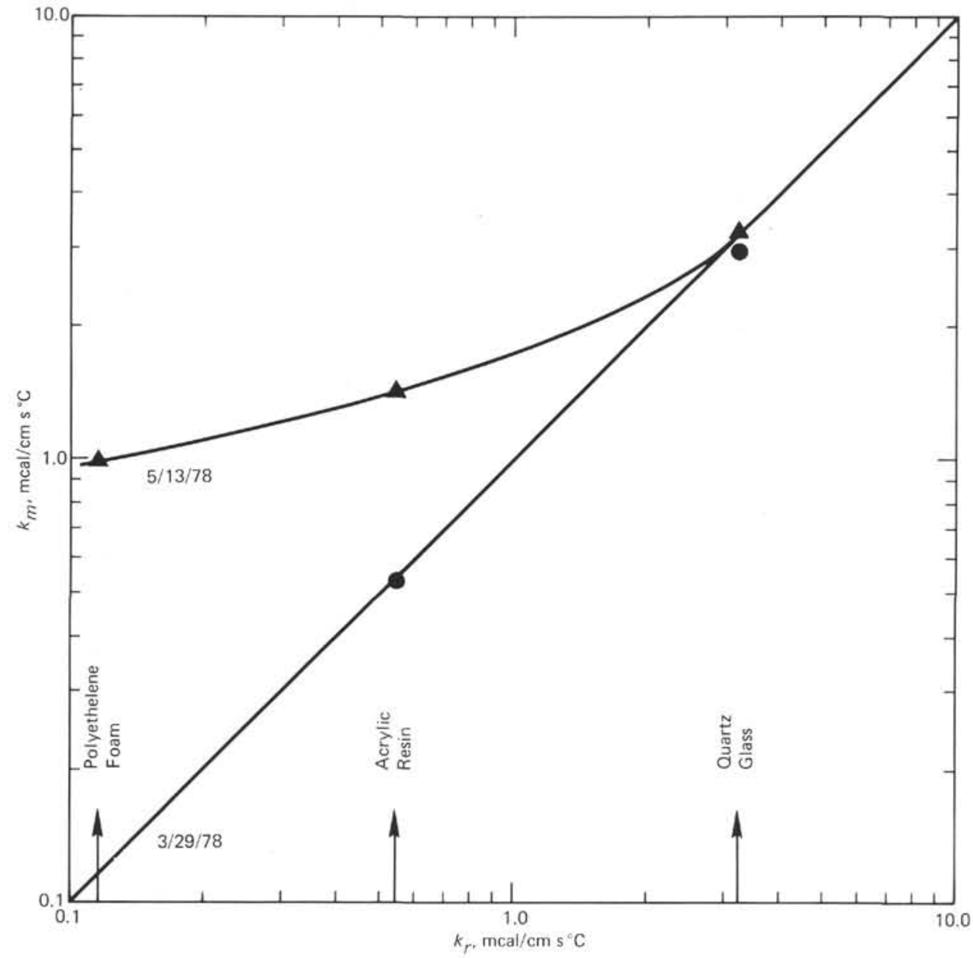

Figure 2. Thermal conductivity k_m measured by the QTM on reference material compared with standard thermal conductivity value k_r of the reference material. Two sets of measurements, repeated by a time span of 45 days, show considerable instrumental drift in the sample thermal conductivity range of $k < 3.22$ mcal/cm s °C, attributed to wear of QTM probe cover.

Site 452

Two short holes were drilled at Site 452. Thermal conductivity was determined on 18 soft sediment samples, mostly pelagic clay, collected from Hole 452 and 12 from Hole 452A drilled to sub-bottom depths of 28.0 and 46.5 meters, respectively. All these measurements were made with the QTM instrument set to the low mode of operation. The thermal conductivity values were corrected according to formula (1) and are summarized in Table 1.

The average and standard deviation calculated from all determinations were 2.15 ± 0.12 mcal/cm s °C for Hole 452 and 2.21 ± 0.18 mcal/cm s °C for Hole 452A.

Table 1. Sample thermal conductivity averaged for the core and the sub-bottom depth of the sample collection, Site 452.

Core	Sub-bottom Depth z (m)	Thermal Conductivity $k \pm \Delta k$ (s.d.) (mcal/cm s °C)	Number of Measurements n
Hole 452			
1	4.50	2.24 ± 0.16	6
2	13.75	2.10 ± 0.06	12
Hole 452A			
1	4.25	2.08 ± 0.19	3
2	13.25	2.11 ± 0.07	3
3	22.75	2.31 ± 0.16	6

Site 453

At Site 453 penetration was 605 meters sub-bottom. The thermal conductivity was measured on 28 soft sediment, 128 semilithified and lithified sediment, and 141 basement rock samples. Both the NP and the QTM were used as the method of measurement.

Table 2A summarizes the result. In calculating the average thermal conductivity for each core, each determination was considered as an individual datum. Therefore, the samples for which the thermal conductivity was determined by both the NP and the QTM were assigned a weight twice that of the samples measured by only one method. The average thermal conductivity is plotted in Figure 3 against the sub-bottom depth. For both the full and partially full cores, the middle of the coring interval was adopted as the depth of the average

Table 2A. Sample thermal conductivity averaged for the core and the sub-bottom depth of the sample collection, Hole 453.

Core	Sub-bottom Depth z (m)	Thermal Conductivity $k \pm \Delta k$ (s.d.) (mcal/cm s °C)	Number of Measurements n
1	4.50	1.96 ± 0.07	6
2	13.75	1.96 ± 0.03	4
3	23.25	2.10 ± 0.11	2
4	32.75	1.87 ± 0.08	5
5	42.25	1.83 ± 0.04	2
6	51.75	1.73	1
8	70.75	1.80 ± 0.08	4
9	80.25	1.89	1
10	89.75	1.82 ± 0.08	3
11	99.25	2.07 ± 0.74	9
13	118.25	1.98	1
14	127.75	2.04 ± 0.24	3
15	137.25	2.17 ± 0.16	3
17	156.25	2.09	1
18	165.75	2.00 ± 0.05	7
20	184.75	2.13 ± 0.21	3
21	194.25	2.49 ± 0.55	4
22	203.75	1.98 ± 0.02	2
23	213.25	2.32 ± 0.37	4
24	222.75	2.21 ± 0.18	4
25	232.25	2.44 ± 0.37	2
26	241.75	2.40 ± 0.29	9
27	251.25	2.65 ± 0.30	6
28	260.75	2.21 ± 0.08	2
29	270.25	2.51 ± 0.20	5
30	279.75	2.64	1
31	289.25	2.59 ± 0.16	3
32	298.75	2.42 ± 0.47	3
33	308.25	3.05 ± 0.60	3
34	317.75	2.43 ± 0.02	3
35	327.25	2.55 ± 0.12	5
36	336.75	2.32 ± 0.13	8
37	346.25	2.58 ± 0.26	6
38	355.75	2.21	1
39	365.25	2.26 ± 0.15	3
40	374.75	2.18 ± 0.02	4
41	384.25	2.73 ± 0.54	7
42	393.75	3.17 ± 0.82	3
43	403.25	2.53	1
44	412.75	2.31 ± 0.31	3
45	422.25	2.83 ± 0.10	5
46	431.75	2.91	1
47	441.25	3.02 ± 0.23	3
48	450.75	3.05	1

thermal conductivity. The plot shows a monotonically increasing thermal conductivity with the sediment depth. The least-square fit of a straight line to the data gives the rate of thermal conductivity increase with depth as (0.23 mcal/cm s °C)/100 m.

"Basement," consisting of a coarse gabbro metabasalt polymict breccia, was encountered 455 meters below the seafloor. Thermal conductivities determined by the high-mode QTM were classified according to the rock types, and the average and standard deviation of the measured thermal conductivities were calculated for each of the rock types as summarized in Table 3. The data were used to estimate the thermal conductivity of the core. The rock-type abundances in Table 4, evaluated visually from the total sample length in the split core samples, represent the rock-type volume fraction in each of the core sections. From these and the rock-type average thermal conductivities, the thermal conductivity of the core was estimated by the method of Horai and Baldridge (1972). The method, originally developed for calculating the thermal conductivity of a rock sample from its mineral composition, is appropriate for estimating the thermal conductivity of the core from its rock composition. The estimated thermal conductivities are shown in Table 4 for all basement core sections. They are arithmetically averaged for each core (Table 2B) and are plotted in Figure 3.

Table 2B. Estimated thermal conductivity for the core and the average sub-bottom depth of the coring interval, Hole 453.

Core	Sub-bottom Depth z (m)	Thermal Conductivity $k \pm \Delta k$ (s.d.) (mcal/cm s °C)	Number of Core Sections n
49	460.25	5.69 ± 0.45	3
50	469.75	5.92 ± 0.47	2
51	479.25	5.29 ± 0.16	4
52	488.75	5.46 ± 0.40	2
53	498.25	5.37 ± 0.18	5
54	507.75	5.31 ± 0.18	3
55	517.25	5.56 ± 0.24	4
56	526.75	5.79 ± 0.52	2
57	536.25	5.54 ± 0.25	4
58	545.75	5.02	1
59	555.25	5.14	1
60	564.75	5.46	1
61	574.25	5.14	1
62	583.75	5.02	1
63	593.25	4.17	1
64	601.50	4.15	1

Site 454

Two holes were drilled at Site 454. Hole 454 reached a sub-bottom depth of 38 meters. Both the NP and the QTM were used for the measurement of thermal conductivity on all 22 soft sediment samples collected from a sub-bottom depth interval between 10 and 37 meters. Hole 454A, drilled nearby, reached a sub-bottom depth of 172 meters. Thermal conductivity values of 6 soft sediment samples collected from a depth interval from 0 to 7 meters sub-bottom and 8 samples from 41 to 61 meters were measured by both the NP and the QTM.

Basement was encountered at a sub-bottom depth of 67 meters in Hole 454A. A total of 88 basement rock samples, consisting of 73 basalts and 15 mudstones, were collected and their thermal conductivities measured by the QTM. The basalt samples are classified into two groups, one representing cooling flow units and the other showing pillow structure. Alteration is minor to moderate in all of the basalt samples. The first 8 mudstone samples occur in the sub-bottom depth interval between 96 and 98 meters and the remaining 7 samples were retrieved from depths between 133 and 142 meters.

Table 5 lists the sample thermal conductivities averaged for each core in Holes 454 and 454A. Figure 4 illustrates the thermal conductivity versus sub-bottom depth relationship. Because the drilling at this site was rather shallow, each individual thermal conductivity value was plotted against the depth of sample collection

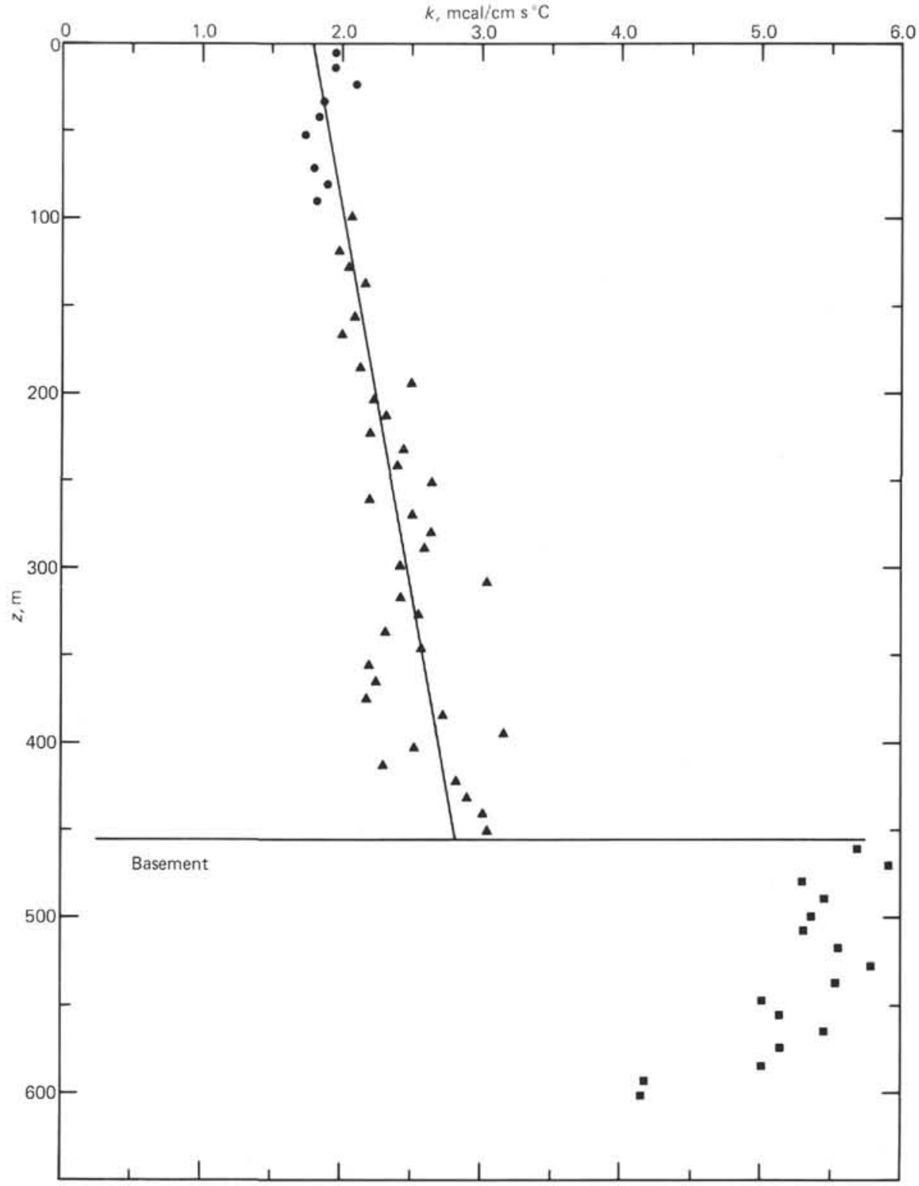

Figure 3. Sample thermal conductivity k averaged for the core plotted against the sub-bottom depth z of sample collection at Site 453. The thermal conductivity of the basement cores is estimated from the rock composition.

Table 3. Thermal conductivity of basement rock samples, Hole 453.

Rock Type	Thermal Conductivity $k \pm \Delta k$ (s.d.) (mcal/cm s °C)	Number of Samples Measured n
Breccia	4.96 ± 0.76	81
Gabbro and norite	6.42 ± 1.21	43
Basalt and diabase	5.46 ± 1.00	13
Serpentinized gabbro and norite	4.15 ± 0.06	3
Mudstone	3.98	1

in order to delineate a detailed distribution of thermal conductivity. The plot revealed that the data for two mudstone layers in the basement are consistent with the distribution of thermal conductivity in the soft sediment stratum. Probably the mudstone samples represent sediment layers buried under the submarine basaltic extrusives, and their thermal conductivity increased as a result of compaction due to loading of the overlying layers. A straight line fit to the sediment thermal conductivity data, inclusive of those two mudstone layers in the basement, gave a rate of thermal conductivity increase with depth (0.28 mcal/cm s °C)/100 m.

The basement basaltic samples show a fairly uniform thermal conductivity. The average and standard deviation of 49 samples from basaltic flow units are 3.96 ± 0.33 mcal/cm s °C and of 24 samples from fragmental pillow basaltic section, 3.39 ± 0.29 mcal/cm s °C. Some basaltic flow unit samples are less vesicular, coarse-grained, and rich in olivine phenocrysts and have thermal conductivities higher than 4.30 mcal/cm s °C.

Table 4. Estimation of basement core/section thermal conductivity from rock composition, Hole 453.

		Constituent Rock and Thermal Conductivity (mcal/cm s °C)				
Core/ Section	Sample Length, Δz (cm)	Gabbro, Norite 6.42	Basalt, Diabase 5.46	Serpentinized Gabbro, Norite 4.15	Breccia 4.96	Estimated Core/Section Thermal Conductivity k (mcal/cm s °C)
49-1	59	0.60	0.20		0.20	5.91
49-2	55	0.13	0.08		0.79	5.17
49-3	22	0.63	0.27		0.10	5.99
50-1	81	0.37	0.19		0.43	5.58
50-2	28	0.85	0.11		0.04	6.25
51-1	83	0.17	0.02		0.81	5.20
51-2	67	0.06	0.19		0.74	5.14
51-3	96	0.23	0.05		0.72	5.30
51-4	97	0.36	0.11		0.53	5.51
52-1	97	0.10	0.16		0.74	5.18
52-2	79	0.55	0.01		0.44	5.74
53-1	105	0.18	0.08		0.74	5.24
53-2	116	0.10	0.23		0.67	5.21
53-3	98	0.42	0.19		0.39	5.64
53-4	107	0.11	0.37		0.52	5.29
53-5	91	0.36	0.04		0.60	5.48
54-1	99	0.13	0.02		0.85	5.15
54-2	105	0.20	0.09		0.71	5.28
54-3	71	0.29	0.29		0.41	5.51
55-1	100	0.27	0.06		0.67	5.36
55-2	107	0.24	0.11		0.65	5.35
55-3	117	0.57	0.03		0.40	5.78
55-4	110	0.56	0.01		0.43	5.76
56-1	86	0.33	0.02		0.65	5.42
56-2	60	0.83			0.17	6.15
57-1	90	0.16	0.18		0.66	5.26
57-3	103	0.59			0.41	5.80
57-4	102	0.53			0.47	5.70
57-5	39	0.33			0.67	5.41
58-1	22		0.35	0.13	0.52	5.02
59-1	11		0.36		0.64	5.14
60-1	4		1.00			5.46
61-1	11		0.36		0.64	5.14
62-1	8		0.13		0.87	5.02
63-1	130		0.02	0.98		4.17
64-1	9			1.00		4.15

Table 5. Sample thermal conductivity averaged for the core and the sub-bottom depth of the sample collection, Site 454.

Core	Sub-bottom Depth z (m)	Thermal Conductivity $k \pm \Delta k$ (s.d.) (mcal/cm s °C)	Number of Measurements n
Hole 454A			
1	5.25	2.26 ± 0.10	6
Hole 454			
3	14.75	2.35 ± 0.13	5
4	24.25	2.15 ± 0.10	9
5	33.75	2.19 ± 0.09	8
Hole 454A			
2	43.25	2.23 ± 0.11	5
3	52.75	2.33	1
4	62.25	2.20 ± 0.04	2
5	71.75	4.15 ± 0.38	19
6	81.25	4.12 ± 0.33	3
8	99.50	2.66 ± 0.64	11
9	108.50	4.03	1
10	117.50	3.52 ± 0.22	4
11	126.50	3.88 ± 0.15	17
12	135.50	3.48 ± 0.45	11
13	144.50	2.73 ± 0.07	5
14	153.50	4.05 ± 0.27	3
15	160.00	4.14 ± 0.06	2
16	166.75	4.04 ± 0.14	9
17	171.50	4.20 ± 0.06	2

Site 455

Hole 455 reached a sub-bottom depth of 104 meters. Soft sediment samples were recovered from depths shallower than 21 meters. Below this level, cores consisted of coarse sand and gravel on which thermal conductivity measurement was impossible.

Table 6 summarizes the results of thermal conductivity measurements. The NP determination gave an average and standard deviation of sample thermal conductivities, 2.57 ± 0.24 mcal/cm s °C (17 samples). This is slightly lower than the result obtained by the QTM of 2.62 ± 0.20 mcal/cm s °C (16 samples).

Site 456

Two holes were drilled at Site 456. The thermal conductivity data are presented separately for each of these holes (Table 7).

Hole 456 reached a sub-bottom depth of 169 meters with basement at 134 meters sub-bottom. A sedimentation hiatus of about 0.7 m.y. separates the unconsolidated (soft) sediment above from the lithified sediment below. Both the NP and the QTM were used for the thermal conductivity measurement on 17 soft sediment samples. Measurement on 17 lithified sediment samples was made by the QTM, with an auxiliary measurement by the NP on one of them.

In Figure 5A, the thermal conductivity is plotted against the depth of sample collection. In the section of soft sediment, the thermal conductivity does not increase with depth. The average and standard deviation are 2.38 ± 0.22 mcal/cm s °C (17 samples by the NP) and 2.59 ± 0.12 mcal/cm s °C (16 samples by the QTM). In the lithified sediment section, the increase of thermal conductivity with depth is apparent. The data, exclusive of one calcareous silty vitric tuff sample with a thermal conductivity of 3.38 mcal/cm s °C, give a rate of (0.67 mcal/cm s °C)/100 m.

Figure 5A also shows the distribution of thermal conductivity in the basement. A sample from a thin layer of limestone at the top of the basement section has a thermal conductivity of 5.06 mcal/cm s °C (by the QTM). Other basement rock samples are basalt. The result of thermal conductivity measurement by the QTM on 28 basalt samples was 4.37 ± 0.31 mcal/cm s °C. The samples with pillow structures indicating their submarine extrusive origin also show moderate to extensive hydrothermal alteration. The degree of alteration is highest in the layer immediately below the limestone and becomes less intensive downward. Correspondingly, the thermal conductivity of the basalt samples is highest near the top of the basement section and decreases in the lower section. Thus the data from the Hole 456 basement provide an example of increasing thermal conductivity with increasing hydrothermal alteration.

Hole 456A was drilled to a sub-bottom depth of 159 m. A thinner lithified sediment section was penetrated in Hole 456A and basement was reached at 114 m sub-bottom. The thermal conductivity was measured on 11 soft sediment, 36 lithified sediment, and 24 basement rock samples. The result is plotted in Figure 5B.

The sediment structure in Hole 456A is similar to that in Hole 456. The thermal conductivity of soft sediment in Hole 456A does not vary with depth. The results of the NP and the QTM measurements were 2.44 ± 0.20 mcal/cm s °C (9 samples) and 2.53 ± 0.12 mcal/cm s

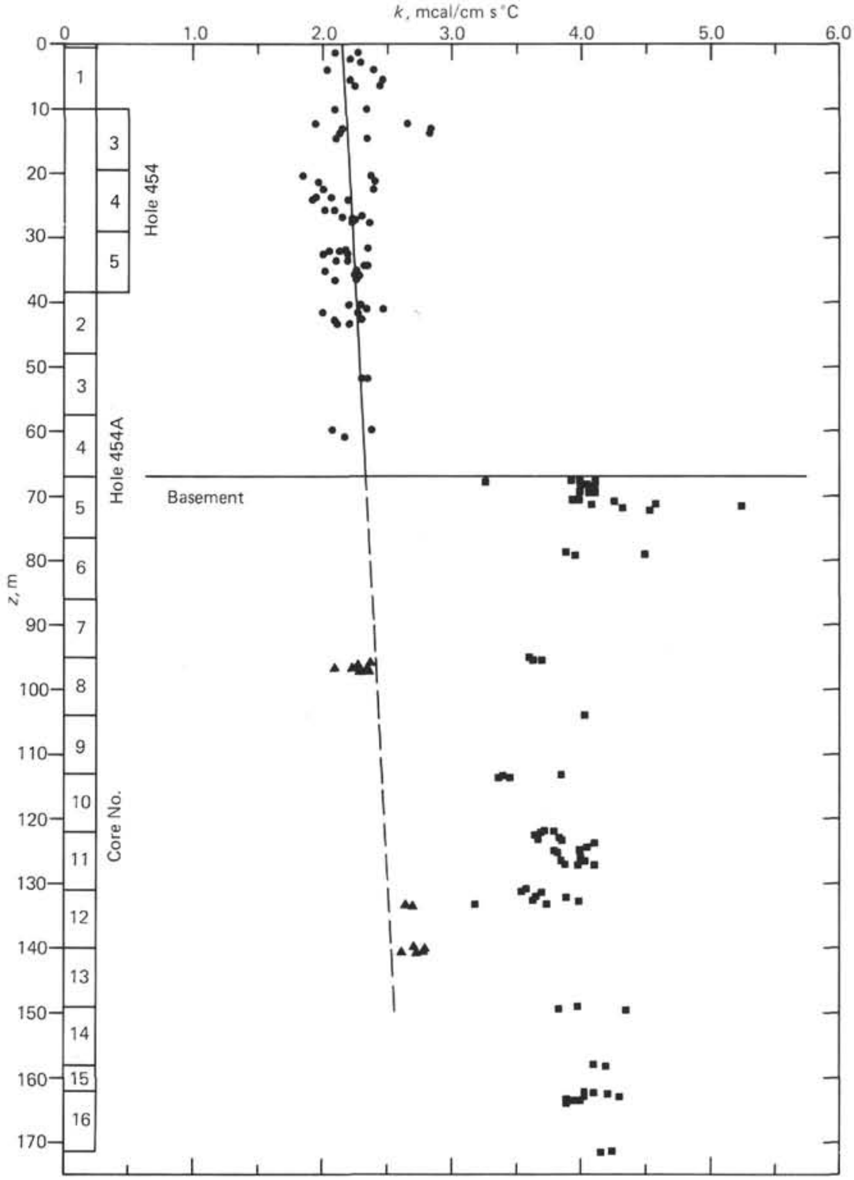

Figure 4. Sample thermal conductivity k plotted against the sub-bottom depth z of sample collection at Site 454.

Table 6. Sample thermal conductivity averaged for the core and the sub-bottom depth of the sample collection, Hole 455.

Core	Sub-bottom Depth z (m)	Thermal Conductivity $k \pm \Delta k$ (s.d.) (mcal/cm s °C)	Number of Measurements n
1	4.50	2.49 ± 0.13	6
2	13.75	2.58 ± 0.21	8
3	23.25	2.79 ± 0.10	3

°C (9 samples), respectively, and are close to the results from Hole 456. The QTM measurement again tends to give a higher thermal conductivity value than the NP.

The thermal conductivity of the lithified sediments increases with depth. Calcareous mudstone and marly chalk samples near the bottom of the sediments have thermal conductivities measured by the QTM ranging from 3.19 to 3.80 mcal/cm s °C. These values deviate from the rest of the data, which indicate a thermal conductivity increase with depth of (0.72 mcal/cm s °C)/100 m.

The rates of thermal conductivity increase with depth —(0.67 mcal/cm s °C)/100 m in Hole 456 and (0.72 mcal/cm s °C)/100 m in Hole 456A—are the highest in all Leg 60 thermal conductivity data. If the sediment lithology change above and below the hiatus is disregarded and a straight line is fitted to the whole sedimentary section, the rate will be (0.56 mcal/cm s °C)/100 m for Hole 456 and (0.59 mcal/cm s °C)/100 m for Hole 456A, still the highest of all Leg 60 determinations. The sediment accumulation rate is also generally high at Site 456. In the lithified sedimentary section the rate is 400 to 1000 m/m.y., the highest of all the

Table 7. Sample thermal conductivity average for the core and the sub-bottom depth of the sample collection, Site 456.

Core	Sub-bottom Depth z (m)	Thermal Conductivity $k \pm \Delta k$ (s.d.) (mcal/cm s °C)	Number of Measurements n
Hole 456			
1	0.25	2.22	1
2	5.25	2.52 ± 0.15	5
3	14.75	2.57 ± 0.11	3
4	24.25	2.67 ± 0.16	2
6	43.25	2.35 ± 0.05	3
7	52.75	2.40 ± 0.09	3
9	71.75	2.86	1
10	81.25	2.72 ± 0.08	6
11	90.75	2.38 ± 0.59	2
12	100.25	2.89 ± 0.10	3
13	109.75	2.84	1
14	119.25	3.09 ± 0.28	2
15	128.75	3.38	1
16	138.25	4.78 ± 0.43	14
17	147.75	4.18 ± 0.26	6
18	157.00	3.89 ± 0.21	5
19	165.25	4.02 ± 0.32	4
Hole 456A			
1	4.75	2.44 ± 0.15	4
3	42.75	2.48 ± 0.18	6
4	52.25	2.49	1
5	61.75	2.70 ± 0.12	5
6	71.25	2.84 ± 0.10	7
7	80.75	2.81 ± 0.12	4
8	90.25	2.98 ± 0.12	4
9	99.75	2.98 ± 0.12	7
10	109.25	3.44 ± 0.18	9
11	118.75	6.04 ± 2.80	3
12	128.25	3.56 ± 0.38	6
13	137.75	3.43 ± 0.34	5
14	147.25	3.62 ± 0.64	6
15	155.50	3.94 ± 0.29	4

determinations made on Leg 60. The association of the highest accumulation rate with the highest thermal conductivity increase with depth will be discussed in detail in a later section.

Rocks constituting basement in Hole 456A are basalt overlain by a layer of carbonaceous sandstone and silicified mudstone. One mudstone sample gave a value of thermal conductivity determined by the QTM of 9.27 mcal/cm s °C. The basalt samples in Hole 456A are distinctively less conductive than those in Hole 456. The measurement result of 23 samples by the QTM was 3.69 ± 0.45 mcal/cm s °C. The basalt samples from Hole 456A are altered, but the degree of alteration is not as intensive as in Hole 456. The data present yet another example of increase in the basalt thermal conductivity as a result of hydrothermal alteration. The precipitation of secondary minerals, as it reduces the porosity of the sample, is undoubtedly responsible for the increase. The effect is further enhanced because secondary minerals crystallized from the hydrothermal fluid consist of such high thermal conductivity minerals as quartz, calcite, or pyrite.

Site 458

At Site 458, a hole was drilled to 466 meters sub-bottom, the upper 256 meters penetrating sediment and the lower 209 meters, basement. The thermal conductivity was measured on 40 soft sediment, 25 lithified sediment, and 184 basement rock samples.

The thermal conductivity of soft sediment samples was determined by both the NP and the QTM. Again the QTM result of 2.63 ± 0.14 mcal/cm s °C for 36 samples was higher than the NP result of 2.46 ± 0.29 mcal/cm s °C for 37 samples. Most thermal conductivity measurements of the lithified sediments were made by the QTM with a few supplementary measurements by the NP. The QTM was used exclusively for the measurement of basement rock samples.

The data were processed in the same fashion as for Site 453. The sample thermal conductivities were averaged for each core, as listed in Table 8, and were plotted against the depth corresponding to the middle of the coring interval (Fig. 6). The sediment thermal conductivity increase with depth is uniform regardless of the sedimentation hiatus of 4 m.y. at sub-bottom depth of 48 meters and the lithology change from soft to lithified sediment at a sub-bottom depth of 143 meters. Near the sediment/basement boundary, the marly chalk samples show distinctively higher thermal conductivities (3.51–4.19 mcal/cm s °C) than the rest of lithified sediment samples. These anomalous data being excluded, the rate of thermal conductivity increase with depth is (0.23 mcal/cm s °C)/100 m, one of the lowest among the determinations made during Leg 60.

At Site 458, the sediment accumulation rate was 6 to 15 m/m.y., the lowest of all Leg 60 determinations. The data complement my earlier observation that a rapid thermal conductivity increase with depth may be related to a high sediment accumulation rate. Later, I shall summarize all data illustrating the relationship between the rate of thermal conductivity increase with depth and the rate of accumulation.

Hole 458 penetrated the basement to a depth of 209 meters below the sediment/basement boundary, the thickest basement section drilled on Leg 60. Thermal conductivity measurements on closely spaced samples collected from the basement cores revealed that the thermal conductivity is correlated with sample texture and degree of alteration, which vary greatly with depth. In Figure 7 the individual sample thermal conductivities were plotted against the depth of sample collection, together with the data on basement rock lithology and porosity.

The Hole 458 basement rock section is divided into five petrologic units. Unit I (Cores 28–31) is a uniform layer of pillowed high-MgO andesite with a constant thermal conductivity of 3.62 ± 0.20 mcal/cm s °C (41 samples). The small variability represents the decrease of vesicularity from pillow rim to interior.

Unit II (Cores 32–37) consists of two massive high-MgO andesite flows. The thermal conductivity is most

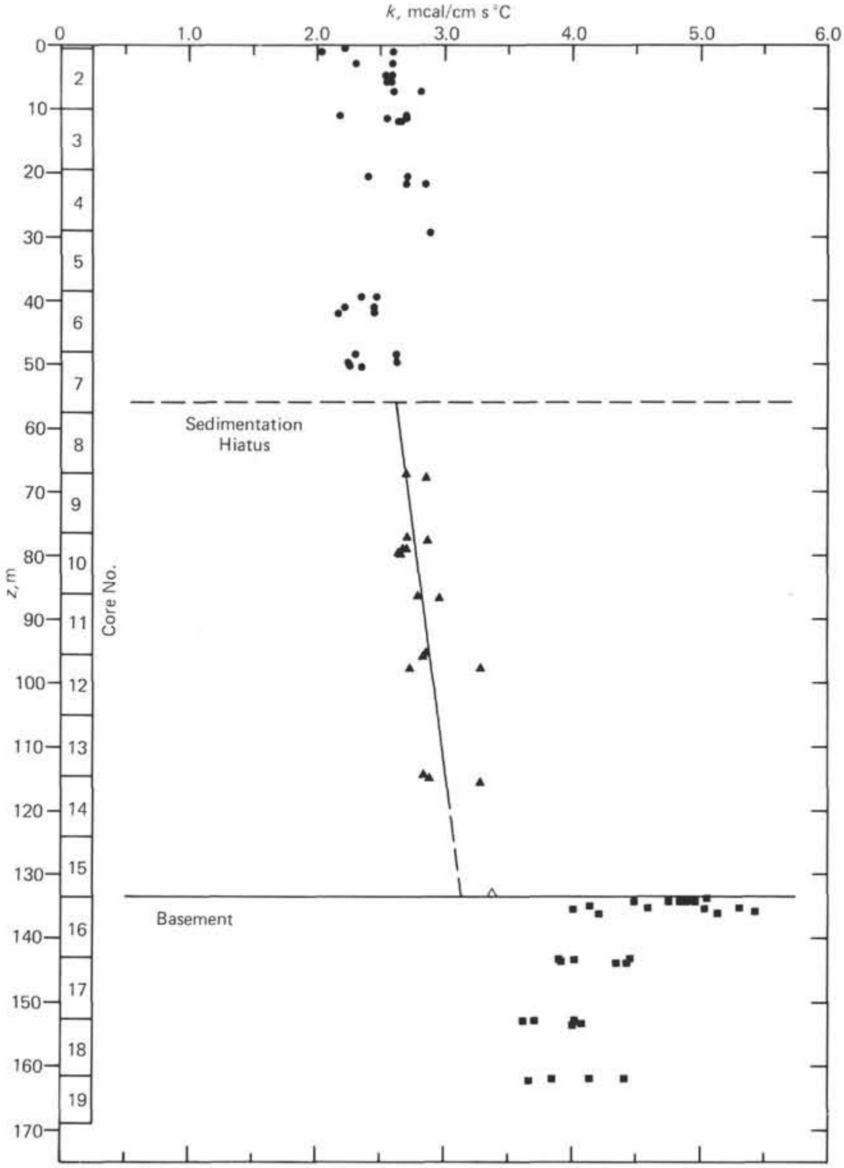

Figure 5A. Sample thermal conductivity k plotted against the sub-bottom depth z of sample collection in Hole 456.

variable in this unit, the average and standard deviation of 58 sample thermal conductivities being 4.38 ± 0.51 mcal/cm s °C. The samples from Core 33, collected from the interior of the first flow unit, where the rock texture is the least vesicular, show the highest thermal conductivities. The thermal conductivity decreases as the samples become more vesicular toward the upper (Core 32) and the lower (Core 34) chilled zones of the flow unit. Samples from the second flow unit (Cores 35–37) show generally lower thermal conductivities. The thermal conductivity of Core 35 samples is maximum at the top of the flow unit and decreases as the samples become progressively more vesicular downward. The intensively fractured and altered samples in Core 36 show the lowest thermal conductivity. The average thermal conductivity of the samples from the lower section of the flow unit (Core 37) is intermediate between those of the upper (Core 35) and the middle (Core 36). The sample texture is vesicular in Core 37 but not as intensively fractured and altered as the samples in Core 36.

Unit III (Cores 38–40) is a mixture of high-MgO andesite pillows and flows. There were at least four flows discernible in its 28.5-meter thickness, indicating that the individual flows are relatively thin. The thermal conductivity, 3.89 ± 0.28 mcal/cm s °C (21 samples), was higher than that of Unit I. The pillowed andesite in Unit III has a mineral composition and texture very similar to that in Unit I. Alteration is, however, more extensive than Unit I. Generally, Unit III samples are less fractured and are thermally more conductive than those in Unit I, probably because the former are less vesicular and hydrothermally more altered.

Units IV (Cores 41–45) and V (Cores 46–49) constitute the lower section of Site 458 basement cores, composed of alternating pillow fragments and fragmented flows. The pillows are usually more vesicular than the

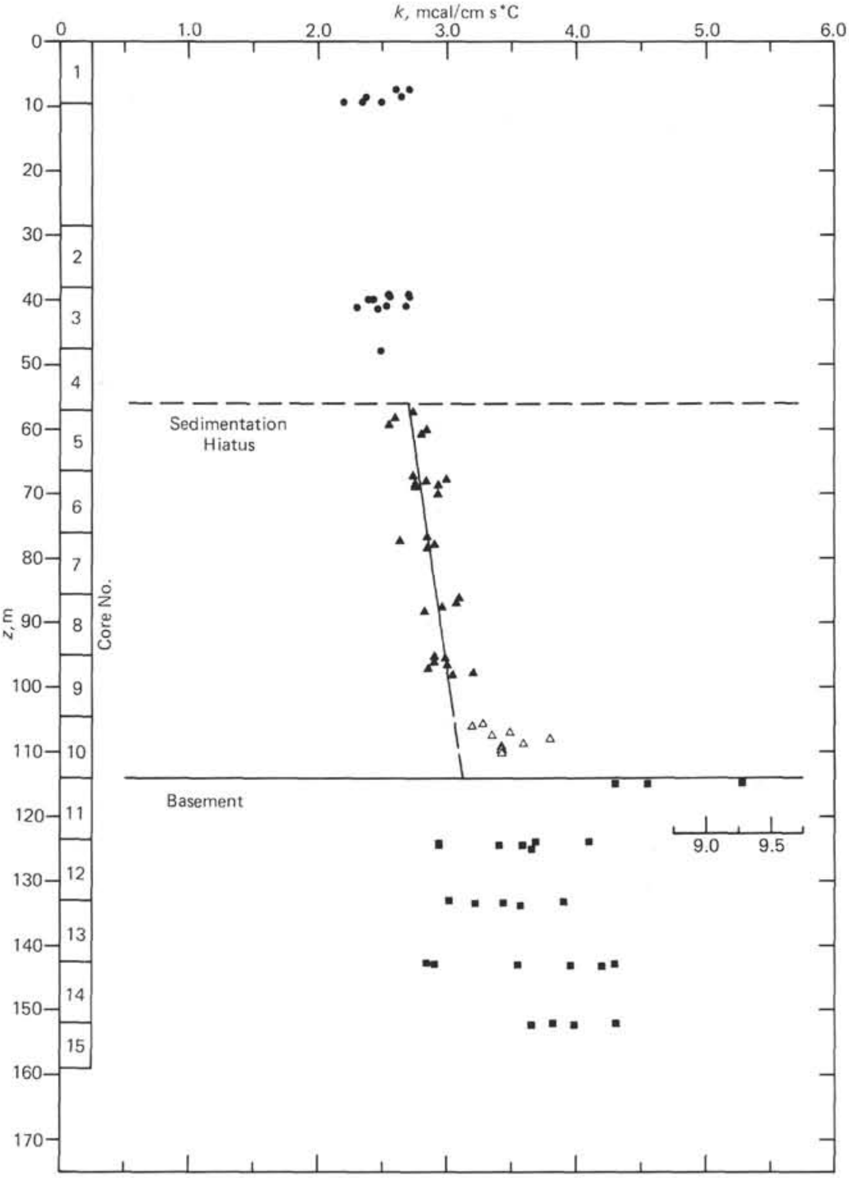

Figure 5B. Sample thermal conductivity k plotted against the sub-bottom depth z of sample collection in Hole 456A.

flows. The flow samples are extensively altered and intensively fractured. A uniform grain-size distribution suggests that the samples of Units IV and V are from the fragmented interior of fairly massive flows. Figure 7 shows that the sample thermal conductivity is uniform in the sub-bottom depth interval corresponding to Units IV and V. The average and standard deviation of sample thermal conductivities is 3.88 ± 0.25 mcal/cm s °C for 37 Unit IV samples and 3.72 ± 0.18 mcal/cm s °C for 21 Unit V samples. No systematic difference exists between the thermal conductivities of pillow and flow samples.

Site 459

Three holes were drilled at Site 459. Hole 459 penetrated only 3.5 meters into the sediment. The thermal conductivity of three soft sediment samples were measured by both the NP and the QTM. Hole 459A reached 67 meters sub-bottom, but no cores were recovered. Hole 459B, the deepest of Leg 60, reached a sub-bottom depth of 692 meters. The sediment section in Hole 459B measured 559 meters and was the thickest of all the sites occupied during Leg 60. Thermal conductivity was measured by both the NP and the QTM on 18 soft sediment, 117 semilithified sediment, and 141 lithified sediment samples from Hole 459B.

The disagreement between NP and QTM measurements was particularly remarkable for the Hole 459B soft sediment samples. The average and standard deviation of 18 measurements were 2.25 ± 0.21 mcal/cm s °C for the NP and 2.74 ± 0.25 mcal/cm s °C for the QTM. For 117 semilithified sediment samples, 83 thermal conductivity measurements were made by the QTM and 38 by the NP. The difference between the results of the NP measurements (2.51 ± 0.25 mcal/cm s °C) and the QTM measurements (3.16 ± 0.15 mcal/cm s °C)

Table 8. Sample thermal conductivity averaged for the core and the sub-bottom depth of the sample collection, Hole 458.

Core	Sub-bottom Depth z (m)	Thermal Conductivity $k \pm \Delta k$ (s.d.) (mcal/cm s °C)	Number of Measurements n
1	4.75	2.55 ± 0.14	6
2	14.25	2.33 ± 0.07	6
3	23.75	2.31 ± 0.08	3
4	33.25	2.51 ± 0.12	4
5	42.75	2.60 ± 0.20	4
6	52.25	2.59 ± 0.14	4
7	61.75	2.61 ± 0.11	5
8	71.25	2.52	1
9	80.75	2.65 ± 0.34	2
11	99.75	2.89 ± 0.26	3
13	118.75	2.58	1
14	128.25	2.52	1
15	137.75	2.66	1
16	147.25	2.74 ± 0.09	3
17	156.75	2.68	1
19	175.75	2.91 ± 0.10	4
22	204.25	2.87	1
24	223.25	3.70 ± 0.11	2
25	232.75	3.82 ± 0.25	8
26	242.25	3.92	1
27	251.75	3.06 ± 0.18	5
28	261.25	3.60 ± 0.26	9
29	270.75	3.55 ± 0.15	19
30	280.25	3.67 ± 0.09	8
31	289.75	3.87 ± 0.23	5
32	299.25	4.62 ± 0.20	17
33	308.75	5.06 ± 0.40	9
34	318.25	4.66 ± 0.16	5
35	327.75	4.06 ± 0.37	11
36	337.25	3.71 ± 0.19	8
37	346.75	4.12 ± 0.20	9
38	356.25	4.39 ± 0.08	3
39	365.75	3.84 ± 0.23	11
40	375.25	3.77 ± 0.11	7
41	384.75	3.71 ± 0.07	7
42	394.25	3.98 ± 0.25	6
43	403.75	3.95 ± 0.28	11
44	413.25	3.99 ± 0.24	5
45	422.75	3.80 ± 0.27	7
46	432.25	3.76 ± 0.15	4
47	441.75	3.68 ± 0.08	11
49	460.75	3.78 ± 0.31	6

cannot be attributed to porewater evaporation. Hole 459B sedimentary cores contain intensely fractured segments. Therefore even in the cores of lithified sediment, the NP measurement was made possible on 14 samples by inserting the needle probe into an intensely brecciated section of the cores. The average and standard deviation of 14 NP measurements, 2.58 ± 0.25 mcal/cm s °C, was significantly different from that of the QTM measurements, 3.20 ± 0.14 mcal/cm s °C, made on the 14 selected samples adjacent to those used for the NP measurements. The total of 127 QTM measurements on lithified sediment samples gave a much higher result: 3.57 ± 0.61 mcal/cm s °C.

It is difficult to determine from an inspection of the cores whether the fracturing is original or is merely the result of drilling disturbance. The results of the NP measurements were not excluded in calculating the average thermal conductivity of the cores in Table 9. The number of NP measurements is relatively small, especially in the deeper sediment section where the disagreement between the two types of measurements becomes more pronounced. The average thermal conductivity of the cores may not be subject to serious error even when the result of the NP measurement does not represent the undisturbed thermal conductivity of the sample. Figure 8 is a plot of the data in Table 9.

The sediment lithology of Hole 459B changes considerably with depth. The upper section (Cores 1–7) consists of vitric, siliceous, calcareous mud and nannofossil vitric ooze. Volcanic ash layers appear in the lower horizon of the section. There are several hiatuses in the sedimentary sequence, all of them shorter than 1 m.y. A major hiatus, about 6 m.y. long, occurs between Cores 7 and 8, separating the upper section from the middle. The middle section (Cores 8–57) is characterized by turbidites. A typical turbidite sequence, from top to bottom, consists of claystone, mudstone, siltstone, and sandstone. Slumping and faulting are common in the turbidite units. Toward the bottom of the section, marly nannofossil limestones are abundant. The lower section (Cores 58 and 59) is separated from the base of the middle section by a 4-m.y. hiatus and is composed of silicified claystone and mudstone intercalated by sandy vitric tuff layers. An 8-m.y. hiatus exists between Cores 58 and 59.

A change of sediment lithology induces a change in thermal conductivity. An example in Figure 9 represents the thermal conductivity measured by the QTM on 10 sediment samples collected from a complete succession of turbidite sequences. The top of the turbidite unit is in Sample 459B-53,CC, which consists of marly nannofossil claystone. Throughout Core 54, Sections 1 and 2, the sample textures are uniform, but their grain size increases slightly downward. The grain size increases to that of siltstone in the lower half of Section 3. Samples of fine- and coarse-grained sandstones appear in Section 4 near the base of the turbidite unit. Figure 9 clearly indicates a downward decrease of the sample thermal conductivity across the vertical section of the turbidite unit. The mechanism for thermal conductivity change with lithology is not fully understood. It is possible that the sample porosity increases downward as a result of grain-size sorting, and this may be the cause of decreasing thermal conductivity. The calcite content of the sediment offers another explanation. Marly nannofossil chalk, constituting the upper section of the turbidite unit, is rich in calcite, which has one of the highest thermal conductivities among the major oceanic sediment constituents. In the lower section, it is replaced by terrigenous sand, poor in calcite. The thermal conductivity of terrigenous sand can be equally high if it contains large amounts of quartz, also one of the highest thermal conductivity minerals. It has been shown, however, that the sand in this particular turbidite unit contains no quartz but feldspar and volcanic glass that have lower thermal conductivities than most of the common rock-forming minerals.

The example given in the foregoing shows that in a small depth interval such as the thickness of a turbidite

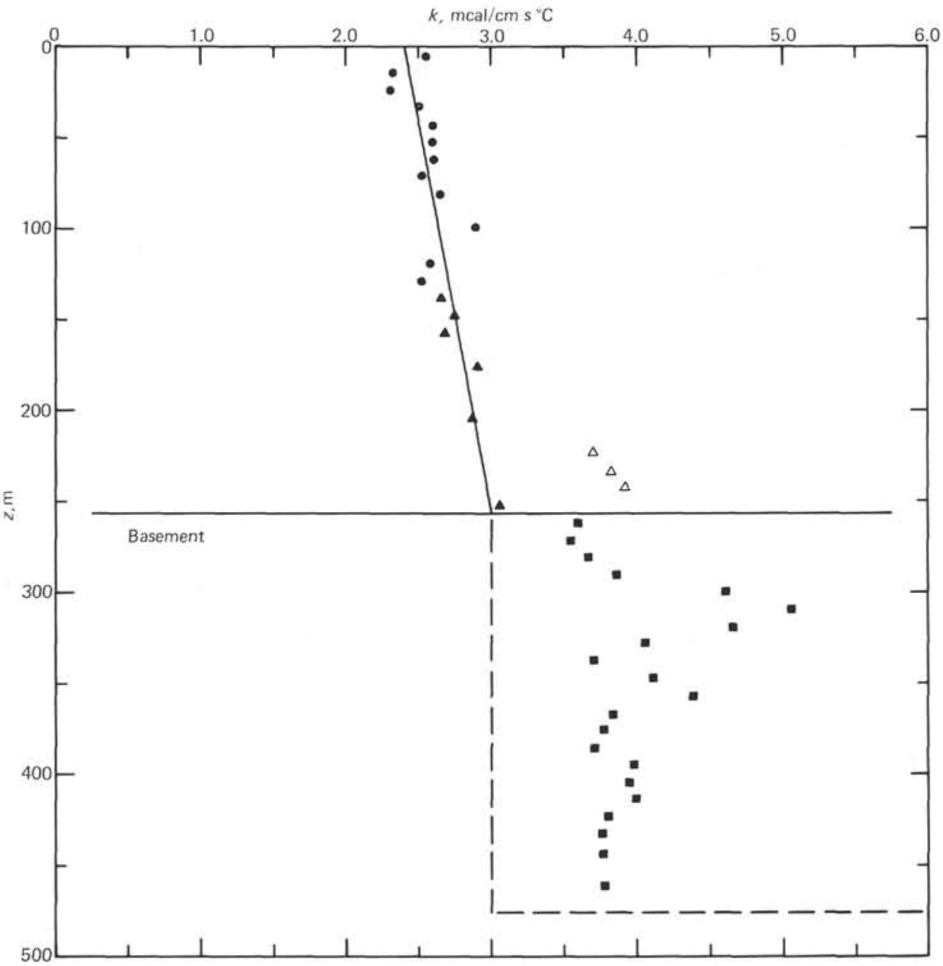

Figure 6. Sample thermal conductivity k averaged for the core plotted against the sub-bottom depth z of sample collection at Site 458. (See Fig. 7 for a detailed distribution of the sample thermal conductivities in the basement.)

unit, thermal conductivity decreases with depth as a consequence of lithologic change. The typical scale length of a single turbidite unit is, however, of the order of a few to several meters. For the whole sedimentary section, the overall lithologic change is such that the degree of sediment compaction and lithification increases with depth. Reflecting this, the data in Figure 8 indicate a general trend of increasing thermal conductivity with depth. Near the bottom of the lithified sediment section, the limestone samples from Cores 55, 56, and 57 have thermal conductivities ranging from 4.89 to 5.56 mcal/cm s °C and deviate conspicuously from the trend suggested by the rest of the data. Excluding these, the increase in sediment thermal conductivity is linear with respect to depth, with a rate of (0.18 mcal/cm s °C)/100 m.

The rate of thermal conductivity increase with depth for Hole 459B sediment was the lowest of all Leg 60 sites. It is even lower than the rate determined by Hyndman et al. (1974) of (0.20 mcal/cm s °C)/100 m for the Leg 26 DSDP holes drilled in the Indian Ocean. The rate of sediment accumulation in Hole 459B ranges from 7 to 52 m/m.y. This is among the lowest of all rates determined in Leg 60 holes. Consequently the data from Hole 459B give another example of a low rate of thermal conductivity increase with depth associated with a low rate of accumulation.

The basement rock samples in Hole 459B are basalt. Some are diabasic in texture. Most of the samples are moderately to extensively altered. Thermal conductivity was measured by the QTM on 73 samples collected from the basement cores. In Figure 10, the individual determinations were plotted against the sub-bottom depth of the sample collection. The variation in the basement rock thermal conductivity correlates remarkably well with the vesicularity (porosity), which varies according to the lithology. The basement section consists of four units. Unit I (Cores 60–62) is an extrusive basaltic flow or a sill intruded along the sediment/basement interface. The thermal conductivity of the basalt samples is low (4.14–4.77 mcal/cm s °C) near the boundary of the flow unit where rock texture is fine grained and vesicular and is high (5.12–5.47 mcal/cm s °C) near the center of the flow unit where the texture is coarse grained and less vesicular. Unit II (Cores 63–65) consists of a sequence of pillow lavas. The thermal conductivity is generally low (3.81–4.33 mcal/cm s °C) and uniform in the unit. The slight increase in thermal conductivity value

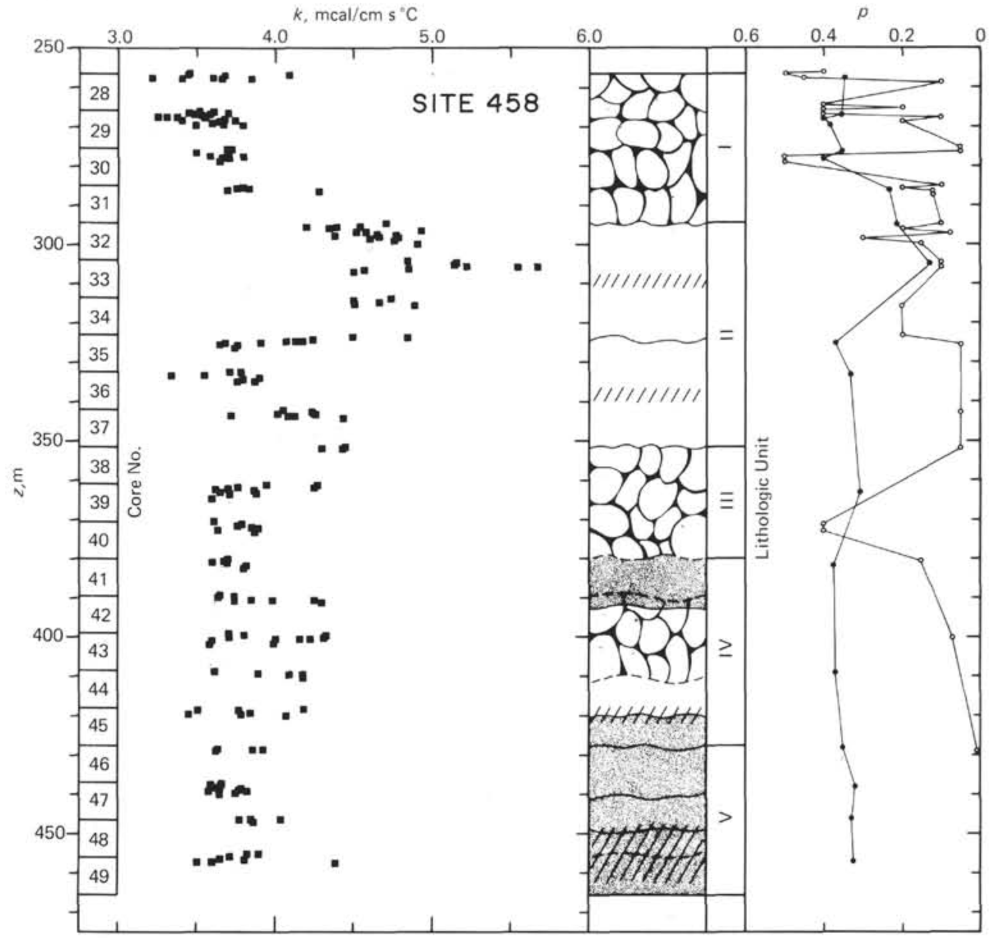

Figure 7. Thermal conductivity k of the basement rock samples plotted against the sub-bottom depth z of sample collection at Site 458. The change of basement lithology and sample porosity (or vesicularity) p as a function of the sub-bottom depth are also shown. The porosity was determined by either wet and dry bulk densities (solid circles) or the point count of petrographic thin sections (open circles).

with depth is probably due to decreasing vesicularity toward the base of the unit. The large glass content (25–90%) in Unit II is also responsible for the lower thermal conductivities. Unit III (Cores 66–68) is a possible sill intruded between the layers of fine-grained basalt (Units II and IV). The samples are medium- to coarse-grained but generally less vesicular than in Unit I. In consequence, these thermal conductivities are the highest (4.19–5.64 mcal/cm s °C) of all four units in Hole 459B basement. Unit IV (Cores 68–73) consists of a sequence of pillow basalt similar to those in Unit II. The Unit IV samples are, however, generally less vesicular than in Unit II. The thermal conductivities are accordingly low to intermediate (3.93–4.93 mcal/cm s °C). The trend of decreasing thermal conductivity with depth is probably due to vesicularity, which on the whole increases toward the base of the unit.

Site 460

Two shallow holes were drilled into a small sediment pond at Site 460. Hole 460 was 85 meters below seafloor. Although basement was not reached, the deepest cores caught fragments of hard rock, which suggests that the sediment layer may be thin. Thermal conductivity was measured on 30 soft sediment samples with results of 2.63 ± 0.32 mcal/cm s °C (27 samples by the NP) and 3.28 ± 0.11 mcal/cm s °C (25 samples by the QTM). The additional QTM measurements on 4 altered basalt samples, probably from the underlying hard rock layer, gave a result of 4.19 ± 0.09 mcal/cm s °C.

Hole 460A penetrated 99.5 meters sub-bottom. Basement sub-bottom depth could not be defined clearly, because the transition from the sediment (Cores 1–8) to the basement (Core 11) was not clear. The results of thermal conductivity measurement on 43 soft sediment samples were 2.59 ± 0.34 mcal/cm s °C (41 samples by the NP) and 3.22 ± 0.32 mcal/cm s °C (36 samples by the QTM). In Hole 460A the conglomerate samples near the base of the sediment section (Cores 8–10) are altered basalt. The samples from the basement (Core 11) are metabasalt. Measurement by the QTM showed that the average thermal conductivity of metabasalt, 5.37 ± 0.40 mcal/cm s °C (5 samples) was decisively higher than that of altered basalt, 3.98 ± 0.08 mcal/cm s °C (7

Table 9. Sample thermal conductivity averaged for the core and the sub-bottom depth of the sample collection, Site 459.

Core	Sub-bottom Depth z (m)	Thermal Conductivity $k \pm \Delta k$ (s.d.) (mcal/cm s °C)	Number of Measurements n
Hole 459			
1	1.75	2.68 ± 0.33	3
Hole 459B			
1	3.75	2.56 ± 0.10	5
2	12.25	2.48 ± 0.15	5
6	50.25	2.36 ± 0.15	6
8	69.25	2.86	1
9	78.75	2.64	1
11	97.75	2.93 ± 0.36	5
12	107.25	2.17	1
13	116.75	2.91 ± 0.32	4
14	126.25	3.06 ± 0.03	4
15	135.75	2.87 ± 0.39	9
17	154.75	3.18 ± 0.01	2
19	173.75	3.14 ± 0.08	2
20	183.25	2.87 ± 0.40	5
21	192.75	2.81 ± 0.46	4
22	202.25	3.04 ± 0.59	3
24	221.25	2.74 ± 0.30	8
25	230.75	2.69 ± 0.32	15
26	240.25	2.73 ± 0.23	5
27	249.75	2.98 ± 0.30	12
28	259.25	3.18 ± 0.21	11
29	268.75	3.08 ± 0.35	10
30	278.25	3.12 ± 0.27	10
31	287.75	3.30 ± 0.24	7
32	297.25	3.07 ± 0.07	5
33	306.75	3.08	1
34	316.25	3.10 ± 0.03	4
35	325.75	3.10 ± 0.07	5
36	335.25	2.76 ± 0.45	5
37	344.75	2.96 ± 0.17	4
38	354.25	2.93 ± 0.29	5
39	363.75	2.99 ± 0.33	3
40	373.25	3.05 ± 0.30	7
41	382.75	3.23	1
42	392.25	3.26 ± 0.09	5
43	401.75	3.33 ± 0.08	2
44	411.25	3.34 ± 0.17	3
45	420.75	3.52 ± 0.15	3
46	430.25	3.34 ± 0.15	5
47	439.75	3.23 ± 0.05	3
48	449.25	3.05 ± 0.43	5
49	458.75	3.50	1
50	468.25	3.42 ± 0.15	7
51	477.75	2.86 ± 0.39	6
52	487.25	3.35 ± 0.11	8
53	496.75	3.47 ± 0.27	9
54	506.25	3.79 ± 0.13	11
55	515.75	(3.40 ± 0.60)[a]	3
		(5.17 ± 0.29)[b]	5
56	525.25	(3.92 ± 0.05)[a]	5
		(5.42 ± 0.09)[b]	4
57	534.75	(3.77 ± 0.08)[a]	4
		(5.51 ± 0.07)[b]	2
58	544.25	3.44 ± 0.09	6
59	553.75	3.87 ± 0.36	4
60	563.25	4.52 ± 0.42	6
61	572.75	5.21 ± 0.22	5
62	582.25	4.89 ± 0.11	2
63	591.75	3.89 ± 0.12	2
64	601.25	4.11 ± 0.32	2
65	610.75	4.16 ± 0.21	2
66	620.25	4.96 ± 0.56	9
67	629.75	4.91 ± 0.32	6
68	639.25	4.70 ± 0.06	4
69	648.75	4.59 ± 0.19	11
70	658.25	4.32 ± 0.37	3
71	667.75	4.46 ± 0.17	7
72	677.25	4.21 ± 0.10	4
73	686.75	4.19 ± 0.15	11

[a] Average for nonlimestone samples.
[b] Average for limestone samples.

samples). Undoubtedly intergranular thermal resistance of the metabasalt was drastically reduced as the result of recrystallization.

For both holes, the difference between the NP and the QTM thermal conductivities of the soft sediment samples was too large to have been caused by porewater evaporation. The Site 460 sediment contains substantial amounts of solid rock fragments such as crystal mud in the upper section, coarse sand in the middle, and pebbles in the lower section of the sediment. The sediment's thermal conductivity increases if it contains solid rock fragments. Because the NP measurement is preferentially made at the spot where the core contains fewer solid rock fragments, it tends to give a lower thermal conductivity than the QTM.

Data on sample density appear to support the foregoing interpretation. The sediment samples from Hole 460A, Core 4 have a GRAPE density ranging from 1.73 to 1.86 g/ml, too high for soft sediment density. If the sample is a mixture of soft sediment (density $\varrho_s = 1.40$ g/ml) and solid rock fragments (density $\varrho_r = 2.10$ g/ml), the volume fraction of solid fragments in the sediment must be between 0.47 and 0.66 to be consistent with the bulk density as indicated in the foregoing. For an assumed thermal conductivity 2.0 mcal/cm s °C of soft sediment and an estimated thermal conductivity of solid rock fragments between 4.6 and 5.1 mcal/cm s °C, the thermal conductivity of the mixture, calculated by the same scheme as for Site 453, agrees with the result of the QTM measurements for the same core, ranging from 3.20 to 3.56 mcal/cm s °C. The estimated solid rock fragment thermal conductivity given in the foregoing is in the range exhibited by Hole 460A hard rock samples—namely, 3.88 to 5.71 mcal/cm s °C. The NP determination of thermal conductivity, though free from the effect of porewater evaporation, is not necessarily more representative than the QTM at Site 460.

The thermal conductivity versus sub-bottom depth data for Holes 460 and 460A (Table 10) indicate an increase of sediment thermal conductivity with depth. The scatter of the data is too large, however, and the depth range of the data distribution too short to give any reliable rate of thermal conductivity increase with depth. Even when the rate can be determined with sufficient accuracy, the increase in thermal conductivity is known due to the increasing volume fraction of solid rock fragments rather than to compaction and lithification of the sediment material. Accordingly, a comparison with the sediment accumulation rate is not meaningful.

Site 461

Two holes were drilled into a shallow sediment pond at Site 461, Hole 461 to 20.5 meters and Hole 461A to 15.5 meters sub-bottom. The soft sediment cores of these short holes caught a number of pebbles. Thermal conductivity was measured on 10 soft sediment samples collected from each hole, with a result similar to that obtained at Site 460. For Hole 461, the average and standard deviation of sample thermal conductivities are 2.38 ± 0.17 mcal/cm s °C (9 samples by the NP) and 3.28 ± 0.16 mcal/cm s °C (9 samples by the QTM). For

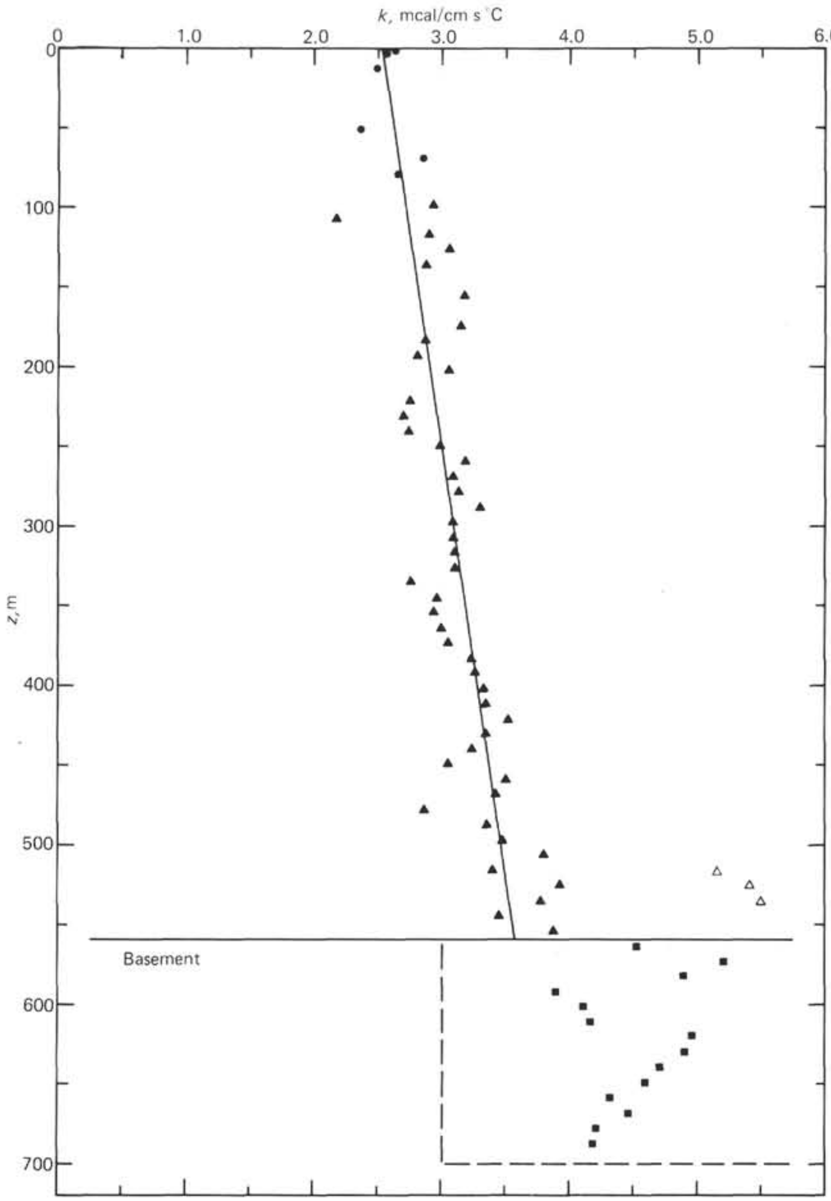

Figure 8. Sample thermal conductivity k averaged for the core plotted against the sub-bottom depth z of sample collection at Site 459. (See Fig. 10 for a detailed distribution of the sample thermal conductivities in the basement.)

Hole 461A, they are 2.56 ± 0.67 mcal/cm s °C (9 samples by the NP) and 3.37 ± 0.28 mcal/cm s °C (10 samples by QTM). The cause of the higher thermal conductivity measured by the QTM and the large differences between the NP and the QTM measurements are thought to be the same as for Site 460.

The pebbles collected from Site 461 consist of a variety of igneous and metamorphic rocks, including basalt, gabbro, diabase, and their metamorphosed facies. The result of thermal conductivity measurement by the QTM was 6.65 ± 0.48 mcal/cm s °C (4 samples) for Hole 461 and 6.04 ± 0.92 mcal/cm s °C (9 samples) for Hole 461A.

Table 11 summarizes the measurement results at Site 461.

DISCUSSION

Relationship between Sediment Thermal Conductivity Increase with Depth and Accumulation Rate

In the foregoing section, some of the site data suggested a correlation between the rate of sediment thermal conductivity increase with depth and the rate of sediment accumulation. Table 12 summarizes the data pertinent to the discussion. They were taken at Sites 453, 454, 456, 458, and 459. Sites 452, 455, 457, and 461 were excluded because the holes drilled at these sites were too shallow to determine any meaningful rate of the sediment thermal conductivity increase with depth; so were the data from Site 460, since we know that the sediment thermal conductivity increase with depth at

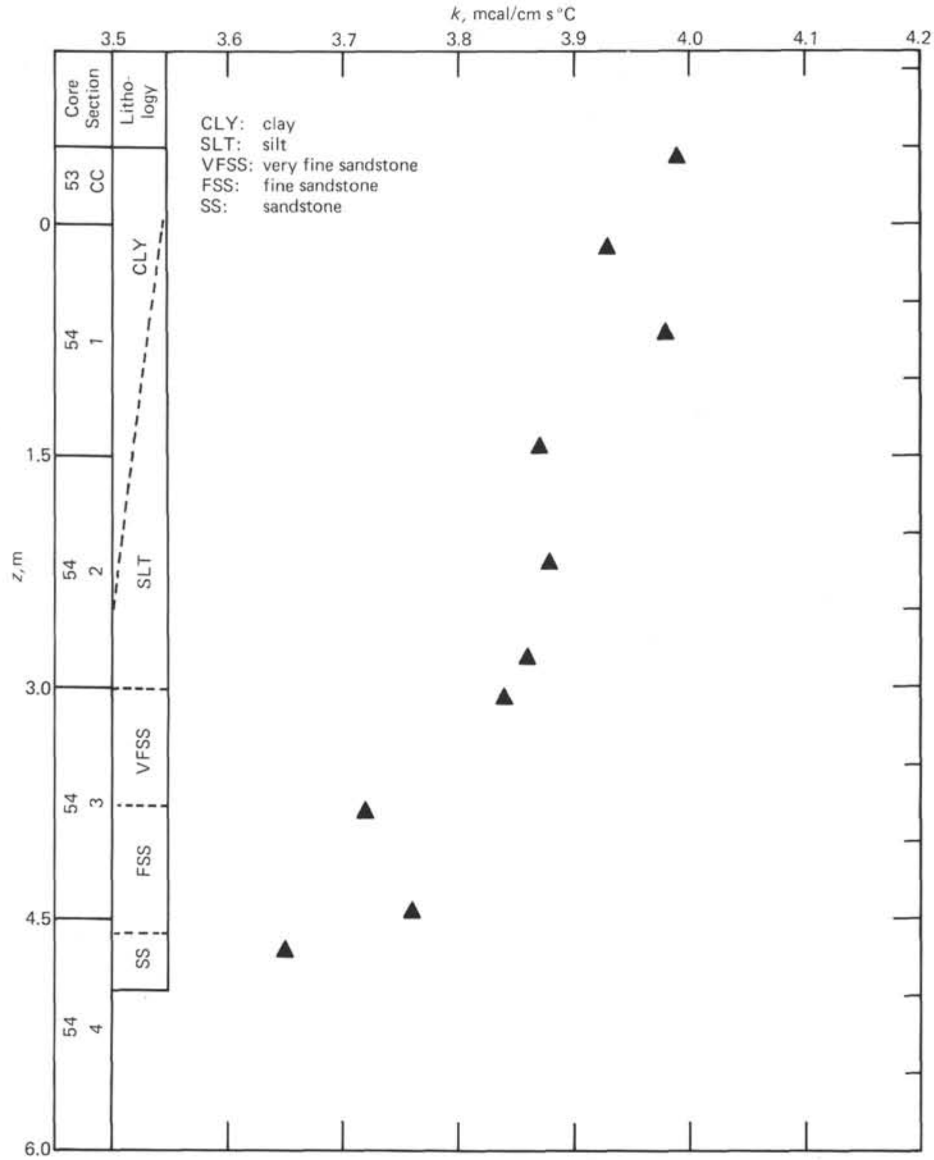

Figure 9. Variation of sample thermal conductivity k along the core length z across the vertical cross section of a turbidite flow unit in Hole 459B, Cores 53 and 54.

this site is due to the increasing content of solid rock fragments in the sediment rather than to compaction and lithification.

The quality of data presented in Table 12 is not uniform. At Sites 453, 458, and 459 the rate of thermal conductivity increase was determined over a sediment depth interval of several hundred meters. At Sites 454 and 456, however, the thermal conductivity data were distributed over a depth interval of only 100 to 150 meters. Obviously more refined data are necessary to establish the suggested relationship. Nonetheless, as illustrated in Figure 11, there appears to be a positive correlation between the rate of thermal conductivity increase with depth and the rate of sediment accumulation.

As noted by Hyndman et al. (1974, 1977), the increase of thermal conductivity with depth is attributed to compaction of sedimentary material. A newly indicated correlation with the rate of sediment accumulation raises the possibility that compaction and lithification of sedimentary material are two competing processes which determine thermal conductivity. Lithification is a uniform rate process that strengthens the bond between the mineral grains. If the sedimentation rate is fast, the sediment material will be compacted prior to the completion of lithification, owing to the compressive load of the rapidly accumulating overlying layers. Conversely, for slowly accumulating sediment, the lithification will be completed while the sediment material has yet to be fully compacted. The lithification increases the thermal conductivity of porous sediment as the intergranular thermal resistance reduces with the cohesion of mineral grains. Obviously, however, the effect is more pronounced in the less porous, compacted sediment. The increase of sediment thermal conductivity with depth is larger for a rapidly accumulating sediment

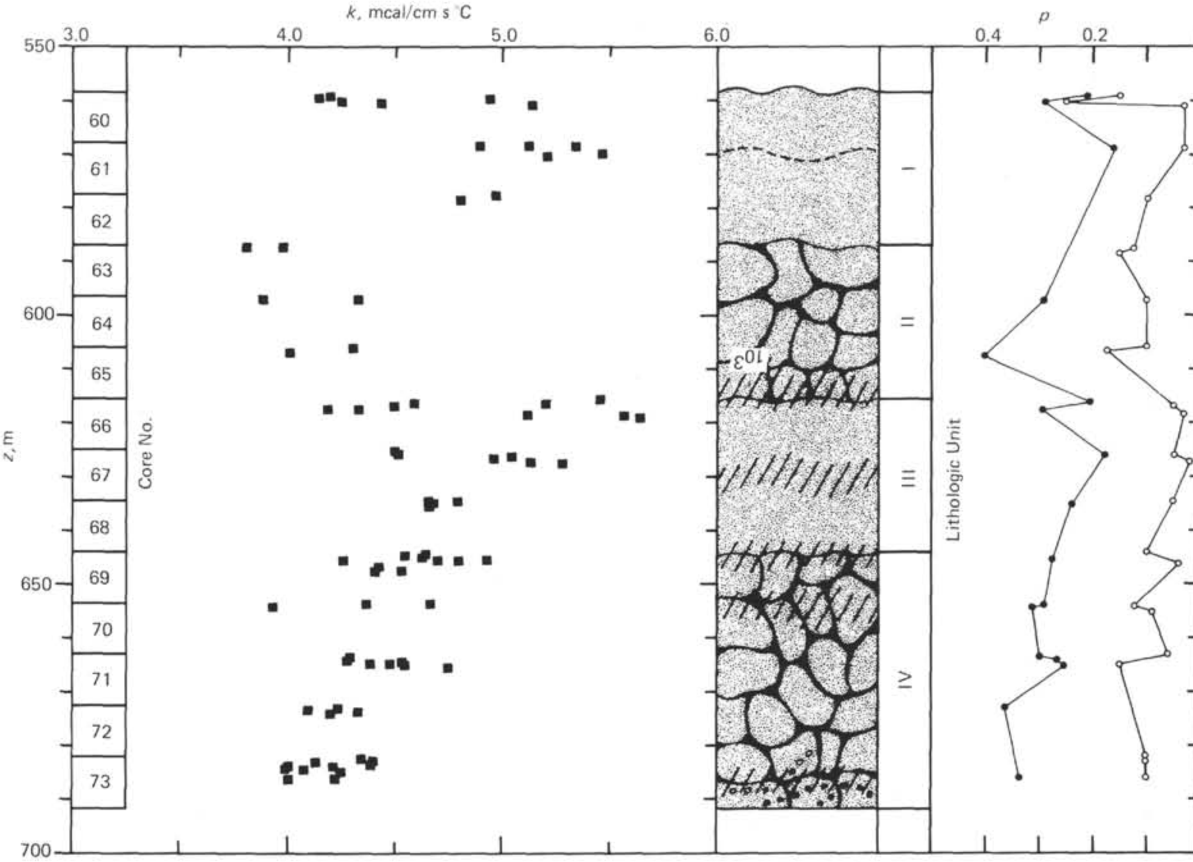

Figure 10. Thermal conductivity k of the basement rock samples plotted against the sub-bottom depth z of sample collection at Site 459. The change of basement lithology and sample porosity (or vesicularity) p as a function of the sub-bottom depth are also shown. The porosity was determined by either wet and dry bulk densities (solid circles) or the point count of petrographic thin sections (open circles).

Table 10. Sample thermal conductivity averaged for the core and the sub-bottom depth of sample collection, Site 460.

Core	Sub-bottom Depth z (m)	Thermal Conductivity $k \pm \Delta k$ (s.d.) (mcal/cm s °C)	Number of Measurements n
Hole 460			
1	4.75	2.87 ± 0.28	10
3	23.75	3.05 ± 0.16	9
4	33.25	2.86 ± 0.20	8
6	52.25	2.64	1
7	61.75	3.69 ± 0.54	3
8	71.25	4.10	1
9	80.75	4.17 ± 0.06	2
Hole 460A			
1	4.00	2.71 ± 0.19	10
2	12.75	2.69 ± 0.36	6
3	22.25	2.74 ± 0.19	6
4	31.75	3.06 ± 0.26	12
5	41.25	3.07 ± 0.32	6
6	50.75	3.02	1
7	60.25	3.44 ± 0.63	3
8	69.75	3.99 ± 0.10	3
9	79.25	3.92 ± 0.04	2
11	98.25	5.37 ± 0.40	5

Table 11. Sample thermal conductivity averaged for the core and the sub-bottom depth of sample collection, Site 461.

Core	Sub-bottom Depth z (m)	Thermal Conductivity $k \pm \Delta k$ (s.d.) (mcal/cm s °C)	Number of Measurements n
Hole 461			
1	0.75	2.40 ± 0.64	2
2	6.25	2.88 ± 0.05	7
3	15.75	5.90 ± 1.73	5
Hole 461A			
1	3.00	3.97 ± 1.59	15
2	10.75	6.22 ± 0.62	4

because the sediment material, lithified after compaction, has a higher thermal conductivity.

Relationship between Surface Sediment Thermal Conductivity and Water Depth

Hyndman et al. (1974) noted from DSDP Leg 26 thermal conductivity data that sediments deposited above the carbonate compensation depth have a higher thermal conductivity than those deposited below it. The

Table 12. The rate of thermal conductivity increase with depth compared with sediment accumulation rate.

Hole	Sub-bottom Depth Range of Data Distribution Δz (m)	Rate of Thermal Conductivity Increase with Depth $\Delta k/\Delta z$ (mcal/cm s °C)/100 m	Rate of Sediment Accumulation $\Delta z/\Delta t$ (m/m.y.)
453	0-456	0.23	20-160
454, 454A	0-149	0.28	90-250
456	67-134	0.67	400-1000
456A	57-105	0.72	
458	0-257	0.23	6-15
459B	0-559	0.18	7-52

difference in thermal conductivity is attributed to the calcite content, which is markedly different above and below the carbonate compensation depth.

Table 13, a summary of Leg 60 data, lists the average thermal conductivity for the top 50 meters of sediment and the depth of water from sea level to the surface of the sediments. A plot of the data in Figure 12 shows that the thermal conductivity decreases linearly as the water depth increases. The thermal conductivity decrease is probably due to the depletion of calcite, one of the most thermally conductive minerals. Accordingly, the relationship can be regarded as a generalization of the results of Hyndman et al. (1974).

The change in pelagic sediment's calcite content with water depth is gradational. Dissolution of calcite begins at the lysocline and continues until, at the carbonate compensation depth, calcite is completely lost. Depths to both the lysocline and the carbonate compensation depth vary according to the ocean. According to Broecker and Takahashi (1977), the lysocline in the north and equatorial Pacific oceans is 3.0 to 3.7 km below sea level and the carbonate compensation depth, 4.0 to 5.0 km; the transition zone from the lysocline to the carbonate compensation depth coincides with the depth range shown in Figure 12.

The surficial thermal conductivity versus water depth relationship is systematically different between the Mariana Arc and Trench area (Sites 452 and 459) and the Mariana Basin (other sites). Perhaps the sedimentary environments are different between these two

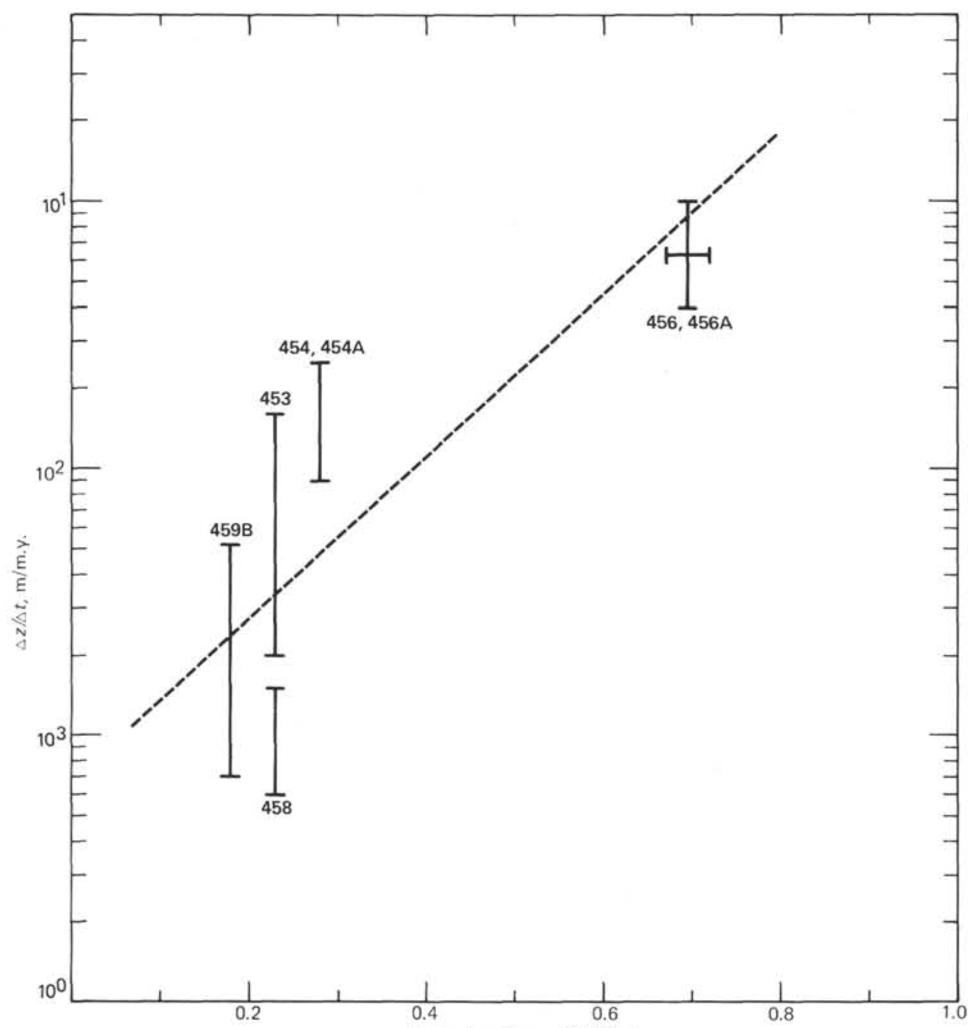

Figure 11. Rate of sediment thermal conductivity increase with depth $\Delta k/\Delta z$ plotted against the sediment accumulation rate $\Delta z/\Delta t$ at Sites 453, 454, 456, 458, and 459 of Leg 60.

Table 13. The sample thermal conductivity averaged for the top 50 meters of sediments compared with water depth.

Hole	Water Depth z (m)	Thermal Conductivity $k \pm \Delta k$ (s.d.) (mcal/cm s °C)	Number of Measurements n
452	5858	2.15 ± 0.12	18
452A	5863	2.21 ± 0.18	12
453	4693	1.93 ± 0.10	21
454, 454A	3819	2.22 ± 0.19	64
455	3468	2.58 ± 0.21	32
456	3591	2.50 ± 0.21	31
456A	3591	2.48 ± 0.17	18
458	3449	2.48 ± 0.23	43
459	4130	2.68 ± 0.36	6
459B	4115	2.49 ± 0.34	28

areas. It is possible that the sediment in the Mariana Arc and Trench area contains more terrigenous material.

Correlation between Thermal Conductivity and Other Physical Properties

Physical properties of the samples (which include soft, semilithified and lithified sediments, and basement rock) such as water content, bulk density, porosity, and compressional sound wave velocity were measured aboard ship. The thermal conductivity was then correlated with these physical properties. These physical property measurements were made on samples which were selected from various locations along the length of the core. They were subsequently classified into four categories according to the distance from the spot of the thermal

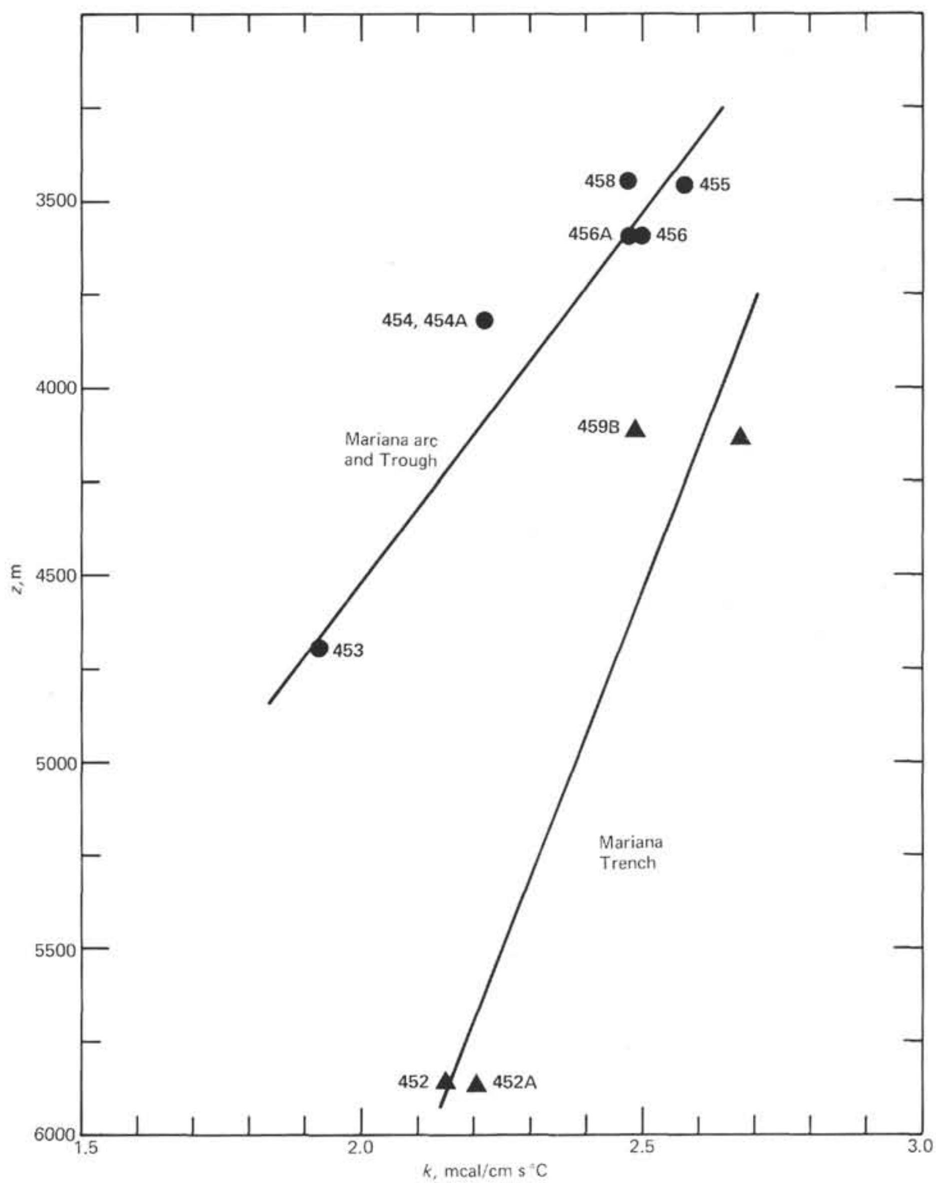

Figure 12. Average thermal conductivity k for the top 50 meters of sediment plotted against the water depth z.

conductivity measurement: within 2.5 cm (Class A), 7.5 cm (Class B), 12.5 cm (Class C), or 17.5 cm (Class D). The analysis showed no distinction among the classes. Class A data did not necessarily give a better correlation with the thermal conductivity than the data of other classes. It was therefore inferred that physical properties are uniform over a distance of 20 cm along the length of the core except where the lithology changes rapidly. In the correlation analysis that follows, I omitted data of physical property separated by more than 20 cm from the location of the thermal conductivity measurement.

Correlation with Water Content

In Figure 13, the thermal conductivity is plotted against water content. If on the same sample the thermal conductivity was determined by both the NP and the QTM, the average of the two measurements is taken. Otherwise, it is the result of either the NP or the QTM measurement. The thermal conductivity of a porous ocean crust sample filled with water decreases monotonically with increasing water content. Ratcliffe (1960) was the first to note that the thermal conductivity of pelagic sediment is a unique function of the water content. Bullard and Day (1961) remarked that the thermal conductivity versus water content relationship can be expressed by a linear equation if, instead of thermal conductivity, its reciprocal (thermal resistivity) is used as a variable. Lachenbruch and Marshall (1966) and Kasameyer et al. (1972) reported data deviating significantly from this relationship and attributed the discrepancy to the anomalous mineral composition of the sediment. Subsequent studies (for example, Popova et al., 1974) showed that frequently the thermal conductivity of pelagic sediment was more adequately represented by Lachenbruch and Marshall's formula than by Bullard and Day's. For comparison purposes, Bullard and Day's and Lachenbruch and Marshall's formulas are illustrated in Figure 13. They are derived from soft sediment thermal conductivity data with water content ranging from 20 to 70% (Bullard and Day) and 30 to 60% (Lachenbruch and Marshall). Within these ranges,

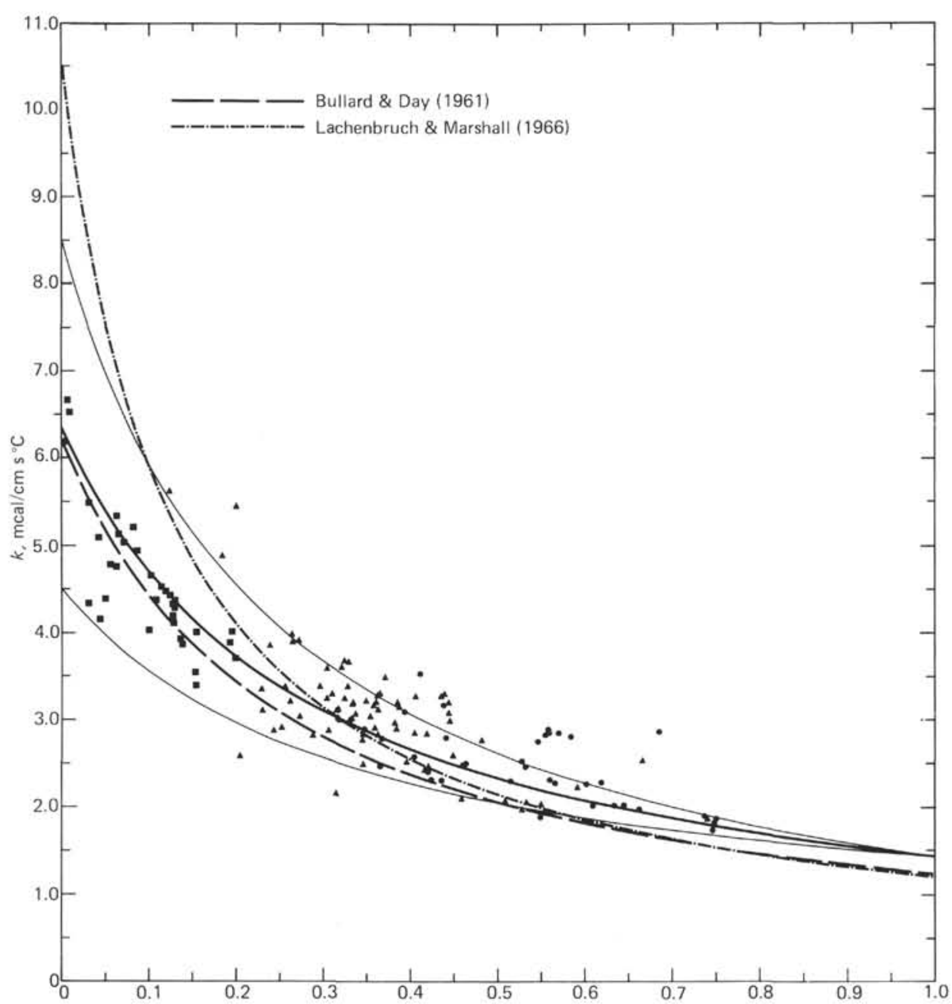

Figure 13. Thermal conductivity k versus water content w plot for Leg 60 ocean crust samples. Data size: n = 145. Curves: ——, best fit to the data (k_s = 6.35 mcal/cm s °C); ——, range of variations corresponding to k_s = 8.50 and 4.50 mcal/cm s °C.

the formulas give systematically lower thermal conductivity values than the Leg 60 soft sediment thermal conductivities. Extrapolated to 100% water content, the respective formulas give 1.20 and 1.23 mcal/cm s °C, too low for the thermal conductivity of seawater at 25°C and 1 atm. The formulas extrapolated to a lower range of water content show, however, a better agreement with the Leg 60 data: Bullard and Day's in the range of 0 to 10% and Lachenbruch and Marshall's from 20 to 30%.

A formula representing the Leg 60 thermal conductivity data over the entire range of water contents was obtained by assuming that the thermal conductivity of a liquid-saturated solid is given by an arithmetic mean of Hashin and Shtrikman's (1962) upper and lower bounds for the thermal conductivity of two-phase material:

$$k = (k_U + k_L)/2, \tag{2}$$

where

$$k_U = k_s + v/[1/(k_w - k_s) + (1 - v)/3k_s]$$
$$k_L = k_w + (1 - v)/[1/(k_s - k_w) + v/3k_w].$$

According to the formula, the thermal conductivity k of an ocean crust sample with its pores filled with seawater is given as a function of the mineral grain thermal conductivity k_s for varying volume fraction v of seawater that has the thermal conductivity k_w. For seawater at 25°C and 1 atm, $k_w = 1.44$ mcal/cm s °C was assumed, and k_s was determined by fitting the formula to the data by the least-squares criterion. The result, $k_s = 6.35$ mcal/cm s °C, will probably be the best estimate of average mineral grain thermal conductivity for Leg 60 samples. The theoretical curve for this value of k_s is illustrated in Figure 13. The deviation of individual data from the curve may reflect varying mineral composition. Figure 13 also shows theoretical curves for $k_s =$ 4.50 and 8.50 mcal/cm s °C that correspond, respectively, to the thermal conductivities of basalt and limestone. A majority of data falls between these two curves, which is consistent with the variety of rock types in Leg 60 ocean crust samples. Some samples show thermal conductivities higher than the theoretical curve for $k_s = 8.50$ mcal/cm s °C. We must keep in mind that dolomite is also a major constituent of ocean sediment. If $k_s = 13.50$ mcal/cm s °C is assumed for the thermal conductivity of dolomite rock, the corresponding theoretical curve coincides with the upper limit of the thermal conductivity in Figure 13. It is possible that some Leg 60 sediment samples are mainly dolomite.

Estimation of Grain Density

The formula used in the foregoing discussion on the analysis of thermal conductivity data contains the volume fraction v as a parameter specifying water content. Because v is not directly measurable, it must be derived from the weight fraction w by the relationship

$$v = w/[w + (1 - w)\,\varrho_w/\varrho_s], \tag{3}$$

where ϱ_w and ϱ_s are the density of seawater and of the mineral grains. We obtained an estimate of ϱ_s in the following way: For a sample of porous material saturated with seawater, the bulk density ϱ is related to ϱ_s, ϱ_w, and w by a formula

$$\varrho^{-1} = \varrho_s^{-1} + w\,(\varrho_w^{-1} - \varrho_s^{-1}). \tag{4}$$

For seawater at 25°C and 1 atm, $\varrho_w = 1.03$ g/ml was assumed, and $\varrho_s = 2.74$ g/ml was determined by fitting Formula 4 to the Leg 60 data illustrated in Figure 14. The small scatter of the data indicates that, despite the varying rock types samples, the average grain density is less variable than any other physical property.

Grain density of porous samples can also be estimated using a relationship between bulk density and porosity p:

$$\varrho = p\,\varrho_w + (1 - p)\,\varrho_s. \tag{5}$$

A fit of Formula 5 to the data of Leg 60 ocean crust samples gave a result of $\varrho_s = 2.77$ g/ml. I conclude that $\varrho_s = 2.75 \pm 0.02$ g/ml would be a reasonable estimate. This value of ϱ_s was used to compute v from w according to Relation 3.

Correlation with Porosity

Porosity p of a porous rock sample is a fractional volumetric ratio of void spaces to total volume. Therefore it is equal to the volume fraction v of water for water-saturated porous rock samples. Because v and water content w are related by Relation 3 and thermal conductivity k is closely related to w as illustrated in Figure 13, it is natural to assume that an equally close relationship exists between k and p. Figure 15 is the k versus p relation based on the data of Leg 60 ocean crust samples.

The figure shows that the thermal conductivity is a monotonically decreasing function of porosity. As in the case of the water content, a formula derived from Hashin and Shtrikman's (1962) theory was used to represent the data. The least-squares analysis was more straightforward than in the previous case, because, as I just noted, porosity is equal to the volume fraction of seawater. The average mineral grain thermal conductivity obtained by the fitting, $k_s = 6.36$ mcal/cm s °C, agrees well with that derived in the previous section from the thermal conductivity versus water content relationship. This expected result demonstrated that bulk density, porosity, and water content data are mutually consistent. In Figure 15 a theoretical curve corresponding to k_s was shown together with those for $k_s = 4.50$ and 8.50 mcal/cm s °C.

The relationship between thermal conductivity and porosity has been studied by several investigators. Robertson and Peck (1974) reported one of the most complete data sets measuring the thermal conductivity of Hawaiian basalt samples under air-filled and water-saturated states. The porosity covered a wide range (2–98%). For comparison, their water-saturated sample

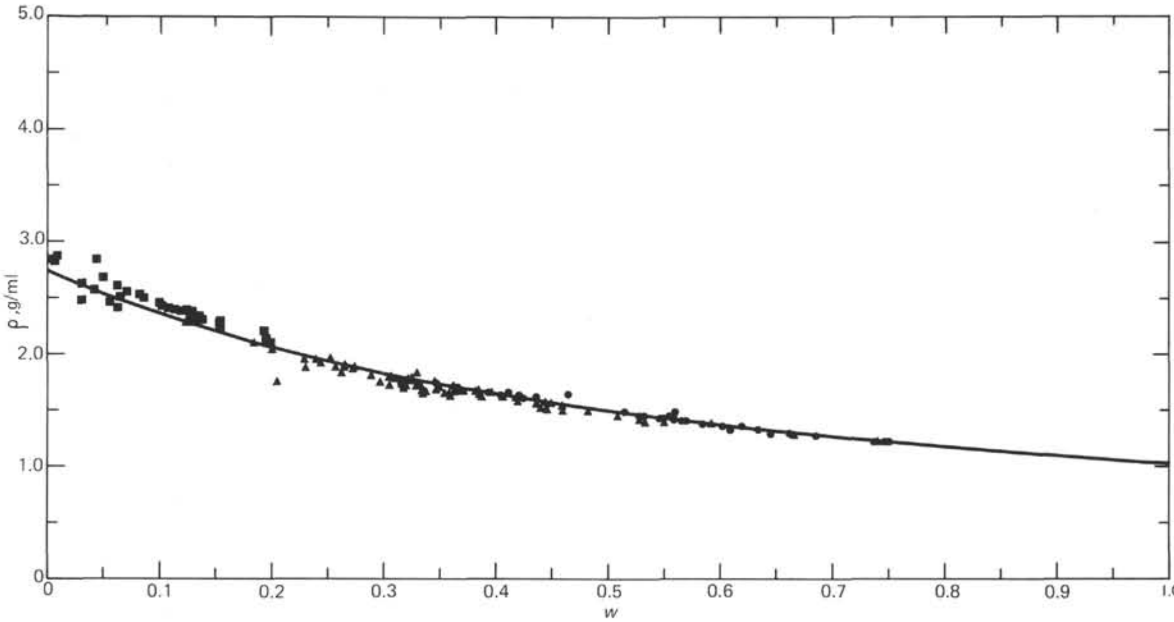

Figure 14. Bulk density ϱ versus water content w plot for Leg 60 ocean crust samples. Data size: n = 145. Curve: ▬▬, best fit to the data (ϱ_s = 2.74 g/ml).

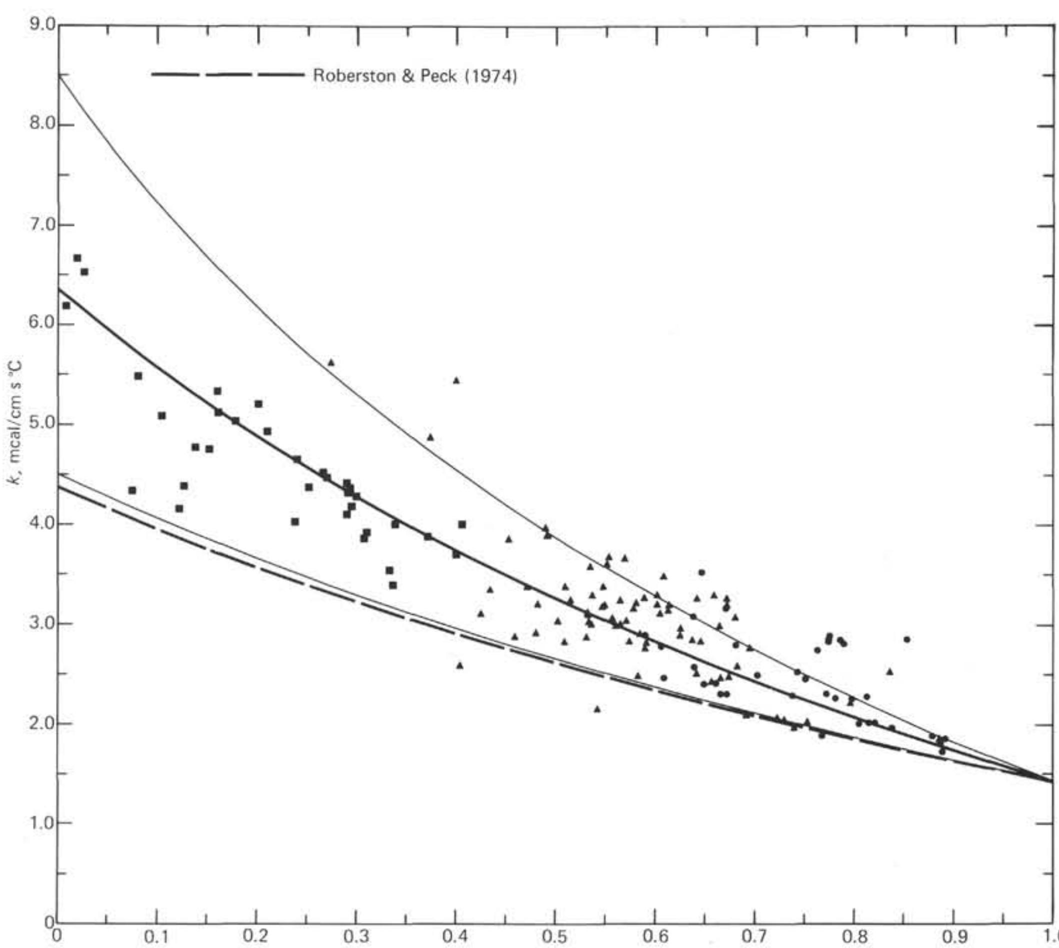

Figure 15. Thermal conductivity k versus porosity p plot for Leg 60 ocean crust samples. Data size: n = 145. Curves: ▬▬, best fit to the data (k_s = 6.36 mcal/cm s °C); ——, range of variations corresponding to k_s = 8.50 and 4.50 mcal/cm s °C.

thermal conductivity versus porosity relationship is reproduced in Figure 15. Instead of displaying the individual thermal conductivity and porosity values, the data were represented by the same formula as I used in my analysis. If $k_s = 4.36$ mcal/cm s °C is assumed, the rms residual between the formula and the data is 0.10 mcal/cm s °C. As noted by Robertson and Peck (1974), the thermal conductivity of the Hawaiian basalt sample increases with increasing olivine content. The samples with a modal olivine content greater than 5% were not included in the data set from which the curve in Figure 15 was calculated. As the figure shows, the theoretical curve corresponding to the value of k_s coincides with the lower limit of Leg 60 ocean crust thermal conductivity. Evidently Leg 60 samples contain minerals with higher thermal conductivities than those in the olivine-free Hawaiian basalt.

Reviewing the site data, I noted that many of the Leg 60 basement rock samples are altered basalt, which tends to show higher thermal conductivities than unaltered basalt. In view of the data in Figure 15, the thermal conductivity increases with alteration not simply because porosity decreases with the deposition of secondary minerals in the samples' voids but, what is more likely, the secondary minerals precipitated from the hydrothermal fluid are of higher thermal conductivities. In fact, the most common secondary minerals in the Leg 60 altered basalt samples, such as quartz, calcite, and pyrite, are thermally more conductive than the rock-forming minerals composing fresh basalt.

Correlation with Bulk Density

Figure 16 is a plot of thermal conductivity versus bulk density for Leg 60 ocean crust samples. Bulk density was determined by two independent methods. Besides measuring mass and volume of a small amount of sample selected from the core, the bulk density was determined continuously along the entire length of the core by the Gamma Ray Attenuation Porosity Evaluator (GRAPE). The GRAPE density usually agrees well with the result of measurements on selected samples, the rms differences between the two measurements being 0.07 g/ml. The results of both measurements were useful in our data analysis. Figure 16 shows a general increase of water-saturated sample thermal conductivity with bulk density.

The relationship between thermal conductivity and density of rock-forming minerals has been studied by Horai and Simmons (1969) and Horai (1971). For the minerals of constant mean atomic weight, the thermal conductivity increases linearly with the density. For the thermal conductivity k in mcal/cm s °C and the density ϱ in g/ml, the proposed relationship was

$$k = (39.0 - 3.25M) + 13.0\,\varrho, \qquad (5)$$

where M is the mean atomic weight. Horai and Baldridge (1972) showed that Relationship 5 is valid not only for silicate rock-forming minerals but for terrestrial igneous and metamorphic rocks as well.

Relationship 5 was derived from the data on pore-free rock-forming minerals and rock samples. The data in Figure 16 are compatible with this relationship if the effect of interstitial water is taken into account. I estimated that the average density of mineral grains for Leg 60 samples is 2.75 g/ml and that thermal conductivity of mineral grains ranges from 4.50 to 8.50 mcal/cm s °C. According to Relationship 5 the corresponding values of M are 20.4 to 21.6, which are reasonable mean atomic weights for calcareous sedimentary and basaltic igneous rocks. If the rock texture is porous and the pores are filled with seawater, the bulk density and thermal conductivity converge to those of seawater at 25°C and 1 atm as the porosity increases. A formula for the thermal conductivity versus density relationship is obtained by eliminating v and w from (2) and (4) with the aid of (3). As illustrated in Figure 16, the formula represents the data satisfactorily. The theoretical curve for $k_s = 6.36$ mcal/cm s °C fits the data best in the sense of minimizing the rms residuals. Its intersection with the vertical line $\varrho = 2.75$ g/ml gives $M = 21.0$, which is regarded as the best estimate of the average mean atomic weight for Leg 60 ocean crust samples.

Correlation with Compressional Sound Wave Velocity

Figure 17 is a plot of the thermal conductivity versus compressional sound wave velocity for Leg 60 ocean crust samples. The compressional sound wave velocity data are the result of routine shipboard measurement on selected core samples by the Hamilton-Frame velocimeter under ordinary laboratory conditions. The plot indicates clearly the increase of compressional sound wave velocity v_p with thermal conductivity k. The functional relationship between v_p and k is, however, totally different from that suggested by Horai and Simmons (1969) and Horai (1971) for a set of pore-free rock-forming minerals.

The effect of interstitital water is again apparent in the data in Figure 17. As with the thermal conductivity, the compressional sound wave velocity of porous, water-saturated samples decreases with porosity. Figure 18 is a compressional sound wave velocity v_p versus porosity p relationship constructed from Leg 60 ocean crust sample data. A theoretical formula to give v_p as a function of p has yet to be developed. The curve in Figure 18 is an empirical fifth-order polynomial fitted to the data by the least-squares method. By eliminating the porosity p (or the water content by volume v) from this expression and Formula 2, a semiempirical relationship between thermal conductivity k and v_p, as illustrated in Figure 17, was obtained.

Figure 18 gives $v_{p,s} = 6.68$ km/s, where $v_{p,s}$, the value of v_p for $p = 0$, is the average mineral grain compressional sound wave velocity corresponding to the average mineral grain thermal conductivity $k_s = 6.40$ mcal/cm s °C. Within the allowable range of uncertainty, these values of $v_{p,s}$ and k_s are consistent with the relationship by Horai and Simmons (1969) and Horai (1971).

$$v_{p,s} = (6.07 \pm 0.17) + (0.15 \pm 0.02)k_s, \qquad (6)$$

which holds for pore-free rocks and rock-forming minerals. With increasing p, both v_p and k of Leg 60 samples approach the sound wave velocity $v_{p,w} = 1.53$

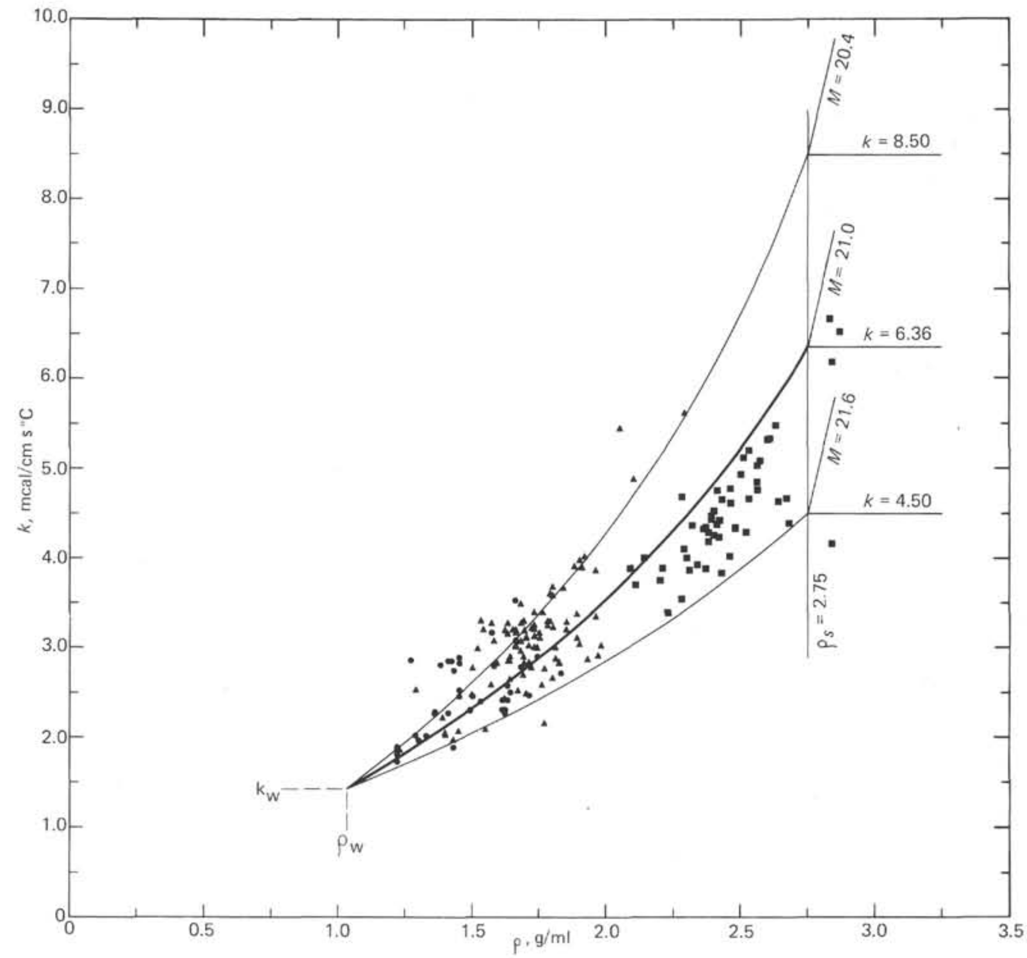

Figure 16. Thermal conductivity k versus bulk density ϱ plot for Leg 60 ocean crust samples. Data size: n = 185. Curves: ▬▬, best fit to the data (k_s = 6.36 mcal/cm s °C); ——, range of variations corresponding to k_s = 8.50 and 4.50 mcal/cm s °C. The relationship among thermal conductivity k, density ϱ, and mean atomic weight M is from Horai (1971).

km/s and the thermal conductivity k_w = 1.44 mcal/cm s °C of seawater at 25°C and 1 atm.

The relationship in Figure 17 is useful in inferring the distribution of thermal conductivity in the ocean crust from the seismic velocity structure. In marine geophysical data interpretation, the Nafe and Drake (1963) relationship has been used for deducing the density structure from that of the seismic velocity. Figure 19 is the v_p versus bulk density ϱ relationship for the data of Leg 60 ocean crust samples. This is not significantly different from that of Nafe and Drake or from a similar relationship by Ludwig et al. (1970) based on more extensive data. Thus, as it appears that Leg 60 ocean crust samples have no local peculiarity, the k versus v_p relationship in Figure 17 will be applicable to most of the world oceans.

CONCLUDING REMARKS

Besides the conventional needle probe technique, the half-space probe technique proved to be an efficient method for thermal conductivity measurements. With appropriate precautions regarding thermal contact at the probe/sample interface, the method was applied successfully to all types of samples (soft sediment, semilithified and lithified sediments, and hard rock) encountered during Leg 60. The new method could be more accurate if, instead of an empirical formula, an exact solution of the thermal conduction equation were used for analysis. The equation to be solved is for an infinite composite solid consisting of two media of different thermal properties separated by a plane boundary, with zero initial temperature and a constant heat emission from a line heat source lying on the interface.

A total of 1547 thermal conductivity values, determined by both the aforementioned methods on 1319 samples drilled during Leg 60, suggested that the rate of sediment thermal conductivity increase with depth may be correlated positively with the sedimentation rate, suggesting that the lithification and compaction are two competing processes determining the thermal conductivity of sediment. Also, the sediment surficial thermal conductivity was found to decrease as the water depth increased from the lysocline to the carbonate compensation depth. The carbonate content in the sediment seems to be an important controlling factor of thermal conductivity. Both relationships need to be firmly estab-

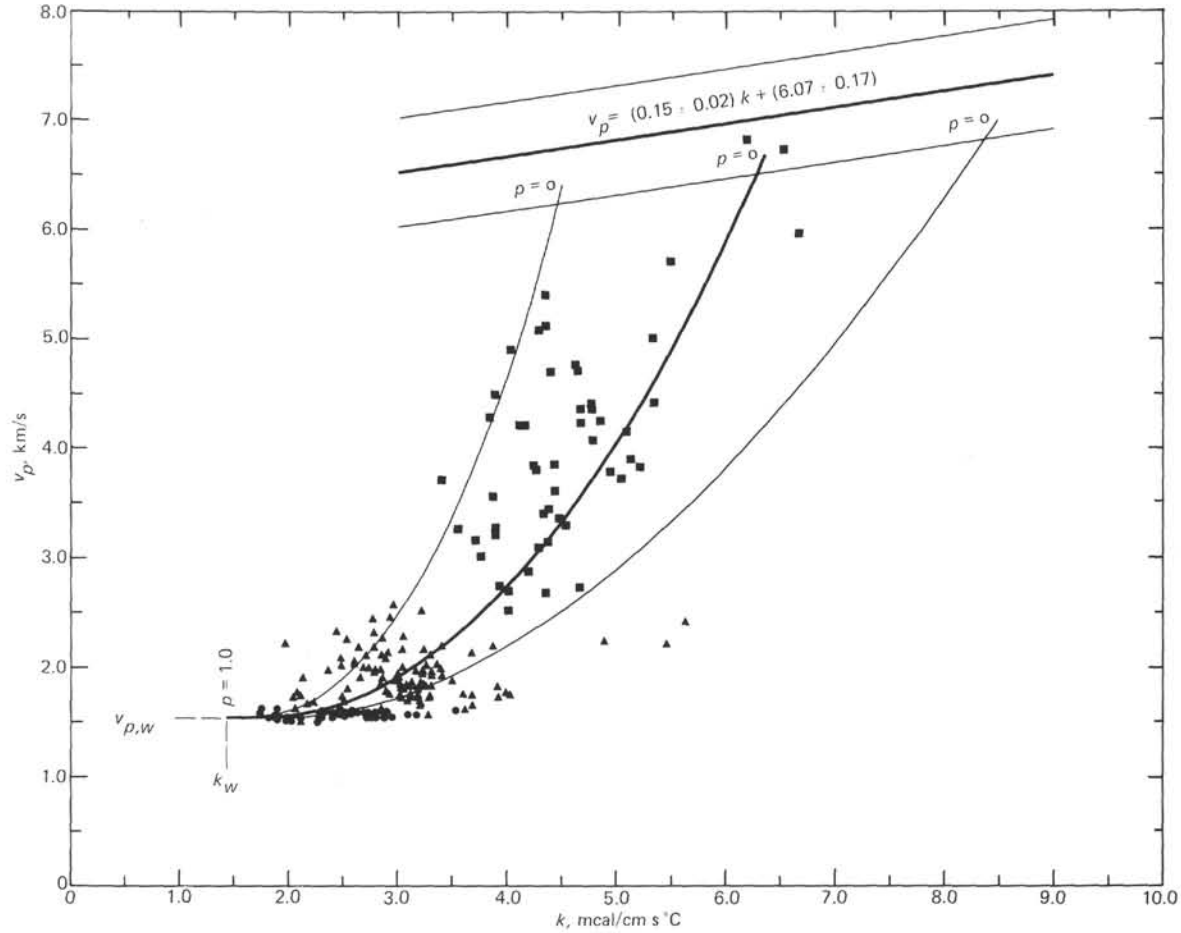

Figure 17. Compressional sound wave velocity v_p versus thermal conductivity k plot for Leg 60 ocean crust samples. Data size: $n = 214$. Curves: ▬▬, best fit to the data (k_s = 6.36 mcal/cm s °C); ——, range of variations corresponding to k_s = 8.50 and 4.50 mcal/cm s °C. Lines: ▬▬, v_p versus k relationship by Horai (1971); ——, range of variations corresponding to the allowances $\Delta k = \pm 0.5$ mcal/cm s °C.

lished by more extensive data. The thermal conductivity of basement rock samples, mostly basalt, is controlled primarily by their vesicularity (porosity). Hydrothermally altered samples tend to show higher thermal conductivities, because minerals precipitated from hydrothermal fluid are thermally more conductive than most common rock-forming minerals. Interdisciplinary study with petrology and petrofabrics is most desirable to confirm this interpretation.

The thermal conductivity versus water content and the thermal conductivity versus porosity relationships were described satisfactorily by a formula based on Hashin and Shtrikman's (1962) variational theory. A single formula was adequate for all types of samples. A second formula representing the thermal conductivity versus compressional wave velocity relationship was obtained by eliminating porosity from the thermal conductivity–porosity formula and an empirical fifth-order polynomial fitted to the wave velocity versus porosity relationship. To unify the theory on the basis of variational principle, a formula similar to Hashin and Shtrikman's must be developed to give compressional sound wave velocity of water-saturated porous material as a function of porosity.

ACKNOWLEDGMENTS

I am indebted to a number of persons for assisting in the present study. Technical assistance by *Glomar Challenger* shipboard technicians Jim Harrington, Don Cameron, Craig Hallman, Richard Myers, and Victor Sotelo was indispensable. Shipboard measurements of the sonic velocity were made by shipboard scientist Tim Francis and that of the water content, bulk density, and porosity by shipboard chemist Jim Pine. Part of the thermal conductivity data was taken by shipboard scientists Tim Francis, Don Hussong, and Seiya Uyeda. The thermal conductivity measurement instrument, Shotherm QTM, was loaned by Showa Denke Co., Ltd., through the courtesy of Mr. Saburo Matsumoto. The needle probe apparatus for the thermal conductivity measurements was designed and constructed—originally to study lunar samples—by the National Aeronautics and Space Administration, L. B. Johnson Space Center technical contractor, Lockheed Electronics Corporation electronics technicians, Charlie Syron and Jerry Winkler. The chapter has been subjected to internal and external reviews. Those who read and constructively criticized the manuscript include Vic Vacquier, Roy Hyndman, Bob Stoll, Mark Langseth, Mike Hobart, Keiko Hattori, Cary Mrozowski, Dallas Abbott and Kerry Hegarty. Joanne Jones and Ginny Rippon are acknowledged for assistance in preparing the manuscript and the figures. Financial support was provided in part by National Science Foundation grant

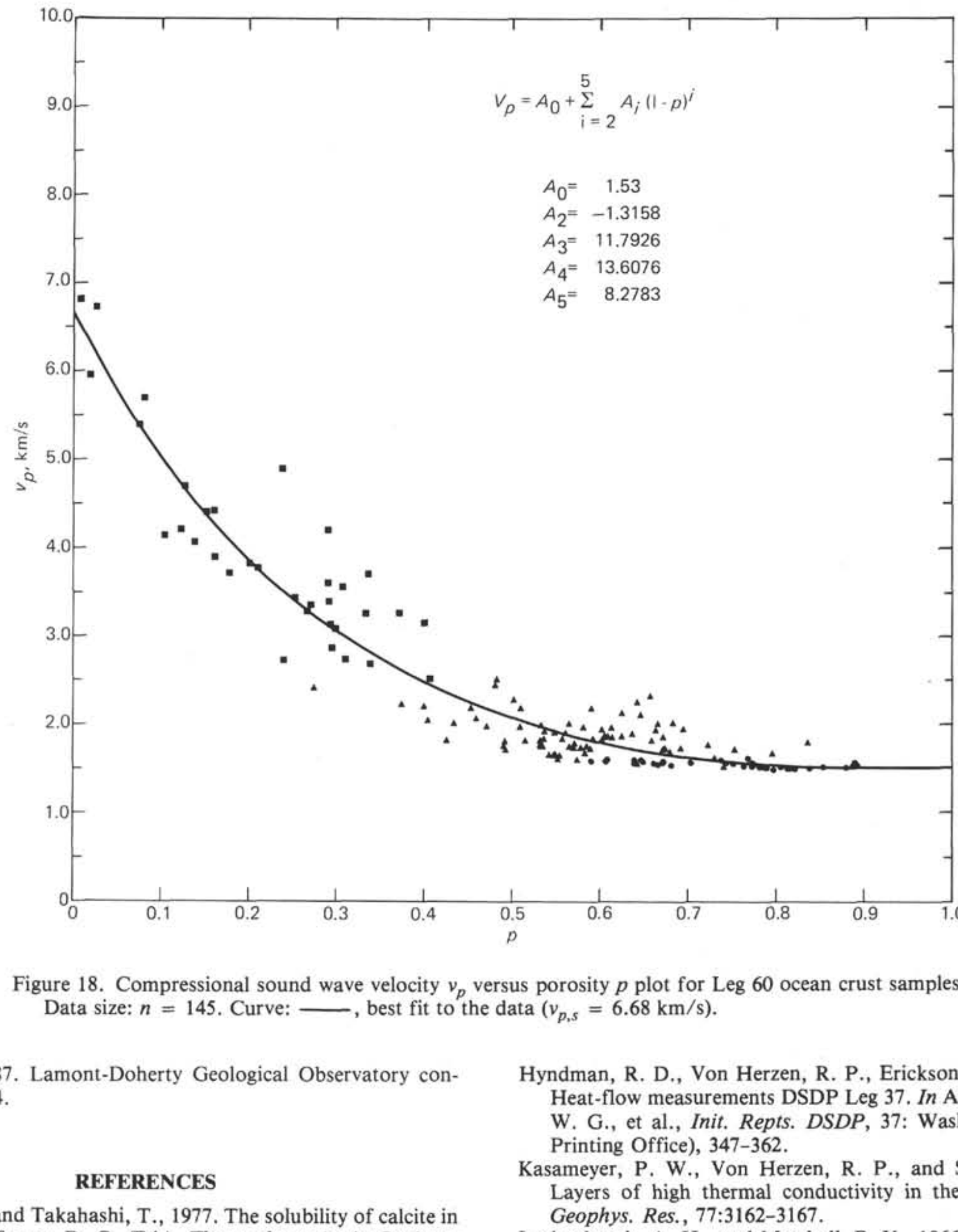

Figure 18. Compressional sound wave velocity v_p versus porosity p plot for Leg 60 ocean crust samples. Data size: $n = 145$. Curve: ——, best fit to the data ($v_{p,s} = 6.68$ km/s).

NSF-OCE-79-19387. Lamont-Doherty Geological Observatory contribution No. 3154.

REFERENCES

Broecker, W. S., and Takahashi, T., 1977. The solubility of calcite in sea water. *In* Frazer, D. G. (Ed.), *Thermodynamics in Geology:* Dordrecht (D. Reidel), pp. 365–379.

Bullard, E. C., and Day, A., 1961. The flow of heat through the floor of the Atlantic Ocean. *Geophys. J.*, 4:282–292.

Erickson, A., 1973. Initial report on downhole temperature and shipboard thermal conductivity measurements, Leg 19, Deep Sea Drilling Project. *In* Creager, J. S., Scholl, D. W., et al., *Init. Repts. DSDP*, 19: Washington (U.S. Govt. Printing Office), 643–656.

Hashin, Z., and Shtrikman, A., 1962. A variational approach to the theory of the effective magnetic permeability of multiphase materials. *J. Appl. Physics*, 33:3125–3131.

Horai, K., 1971. Thermal conductivity of rock-forming minerals. *J. Geophys. Res.*, 76:1278–1308.

Horai, K., and Baldridge, S., 1972. Thermal conductivity of nineteen igneous rocks, 2: Estimation of the thermal conductivity of rock from the mineral and chemical compositions. *Phys. Earth Planet., Inter.*, 5:157–166.

Horai, K., and Simmons, G., 1969. Thermal conductivity of rock-forming minerals. *Earth Planet. Sci. Lett.*, 6:359–368.

Hyndman, R. D., Erickson, A. J., and Von Herzen, R. P., 1974. Geothermal measurements on DSDP Leg 26. *In* Davis, T. A., Luyendyk, B. P., et al., *Init. Repts. DSDP*, 26: Washington (U.S. Govt. Printing Office), 451–463.

Hyndman, R. D., Von Herzen, R. P., Erickson, A. J., et al., 1977. Heat-flow measurements DSDP Leg 37. *In* Aumento, F., Melson, W. G., et al., *Init. Repts. DSDP*, 37: Washington (U.S. Govt. Printing Office), 347–362.

Kasameyer, P. W., Von Herzen, R. P., and Simmons, G., 1972. Layers of high thermal conductivity in the North Atlantic. *J. Geophys. Res.*, 77:3162–3167.

Lachenbruch, A. H., and Marshall, B. V., 1966. Heat flow through the Arctic Ocean floor: The Canada Basin–Alpha Rise boundary. *J. Geophys. Res.*, 71:1223–1248.

Ludwig, W. J., Nafe, J. E., and Drake, C. L., 1970. Seismic refraction. *In* Maxwell, A. E. (Ed.), *The Sea* (Vol. 4): New York (Wiley-Interscience), 53–84.

Nafe, J. E., and Drake, C. L., 1963. Physical properties of marine sediments. *In* Hill, M. N. (Ed.), *The Sea* (Vol. 3): New York (Wiley-Interscience), 794–815.

Popova, A. K., Suvilov, E. A., and Hobart, M., 1974. Geothermal investigation of the mid-Atlantic ridge rift zone. *In* Vinogradov, A. P., and Udintsev, G. B. (Eds.), *Investigation of the Problems Concerning the Rift Zones of the World Oceans* (Vol. 3): Moscow (Nauka), 199–202.

Ratcliffe, E. H., 1960. The thermal conductivities of ocean sediments. *J. Geophys. Res.*, 65:1535–1541.

Robertson, E. C., and Peck, D. L., 1974. Thermal conductivity of vesicular basalt from Hawaii. *J. Geophys. Res.*, 79:4875–4888.

Sumikama, S., and Arakawa, Y., 1976. Quick thermal conductivity meter. *Instru. Autom.*, 4:60–66.

Von Herzen, R. P., and Maxwell, A. E., 1959. The measurement of thermal conductivity of deep-sea sediments by a needle-probe method. *J. Geophys. Res.*, 64:1557–1563.

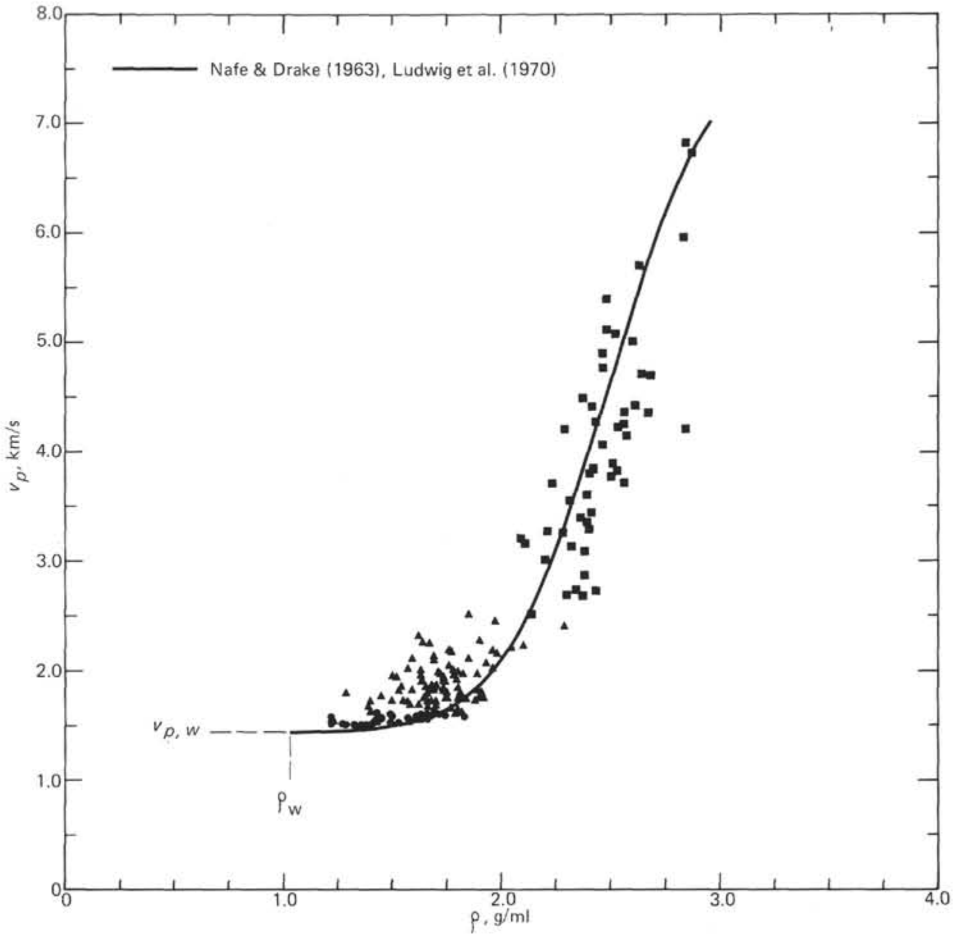

Figure 19. Compressional sound wave velocity v_p versus bulk density ϱ plot for Leg 60 ocean crust samples. Data size = 184.